QUARTERLY JOURNAL
OF THE
ROYAL METEOROLOGICAL SOCIETY

Vol. 126 | JANUARY 2000 Part A | No. 562

Q. J. R. Meteorol. Soc. (2000), **126**, pp. 1–30

A turbulence scheme allowing for mesoscale and large-eddy simulations

By J. CUXART[1]*, P. BOUGEAULT[2] and J.-L. REDELSPERGER[2]
[1]*Instituto Nacional de Meteorología, Spain*
[2]*CNRM/GAME (Météo-France and CNRS), France*

(Received 30 June 1998; revised 30 March 1999)

SUMMARY

The paper describes the turbulence scheme implemented in the Meso-NH community research model, and reports on some validation studies. Since the model is intended to perform both large-eddy and mesoscale simulations, we have developed a full three-dimensional scheme, based on the original method of Redelsperger and Sommeria. A prognostic equation for the turbulent kinetic energy is used, together with conservative variables for moist non-precipitating processes. A particularity of the scheme is the use of variable turbulent Prandtl and Schmidt numbers, consistently derived from the complete set of second-order turbulent-moment equations. The results of three idealized boundary-layer simulations allowing detailed comparisons with other large-eddy simulation (LES) models are discussed, and lead to the conclusion that the model is performing satisfactorily.

The vertical flux and gradient computation can be run in isolation from the rest of the scheme, providing an efficient single-column parametrization for the mesoscale configuration of the model, if an appropriate parametrization of the eddy length-scale is used. The mixing-length specification is then the only aspect of the scheme which differs from the LES to the mesoscale configuration, and the numerical constants used for the closure terms are the same in both configurations. The scheme is run in single-column mode for the same three cases as above, and a comparison of single-column and LES results again leads to satisfactory results. It is believed that this result is original, and is due to the proper formulation of the parametrized mixing length and of the turbulent Prandtl and Schmidt numbers. In fact, a comparison of the parametrized mixing length with the length-scale of the energy-containing eddies deduced by spectral analysis of the LES shows interesting similarity.

KEYWORDS: Ensemble-average scheme Spectral length Subgrid-scale scheme Turbulence Variable turbulent Prandtl numbers

1. INTRODUCTION

The numerical simulation of atmospheric turbulence has been undertaken in the past under two different approaches:

(i) The large-eddy simulation (LES) is performed over small domains with resolutions ranging from centimetres to some tens of metres (Fig. 1(a)). It needs a parametrization of the nonlinear interactions between the subgrid-scale and resolved eddies (SGS, or subgrid turbulence scheme). It is usually assumed that the subgrid-scale eddies are homogeneous and nearly isotropic and can be represented by the Kolmogorov theory (Kolmogorov 1942). The classical scheme of Smagorinsky (1963) is based on this hypothesis and is still widely used. SGS schemes based on the use of a prognostic variable for the turbulent kinetic energy (TKE or e, defined as half the sum of the velocity variances) also use this hypothesis (Lilly 1967). It is well known, however, that the turbulent motions are not isotropic in the presence of stable stratification or near solid boundaries. In the first case, stability functions have been proposed (Lilly 1962), and near the ground some attempts are the backscatter approach (Leith 1990; Mason and Thomson 1992) or

* Corresponding author: Servicio de Modelización Numérica del Tiempo, Instituto Nacional de Meteorología, Camino de las Moreras s/n, 28040, Madrid, Spain.

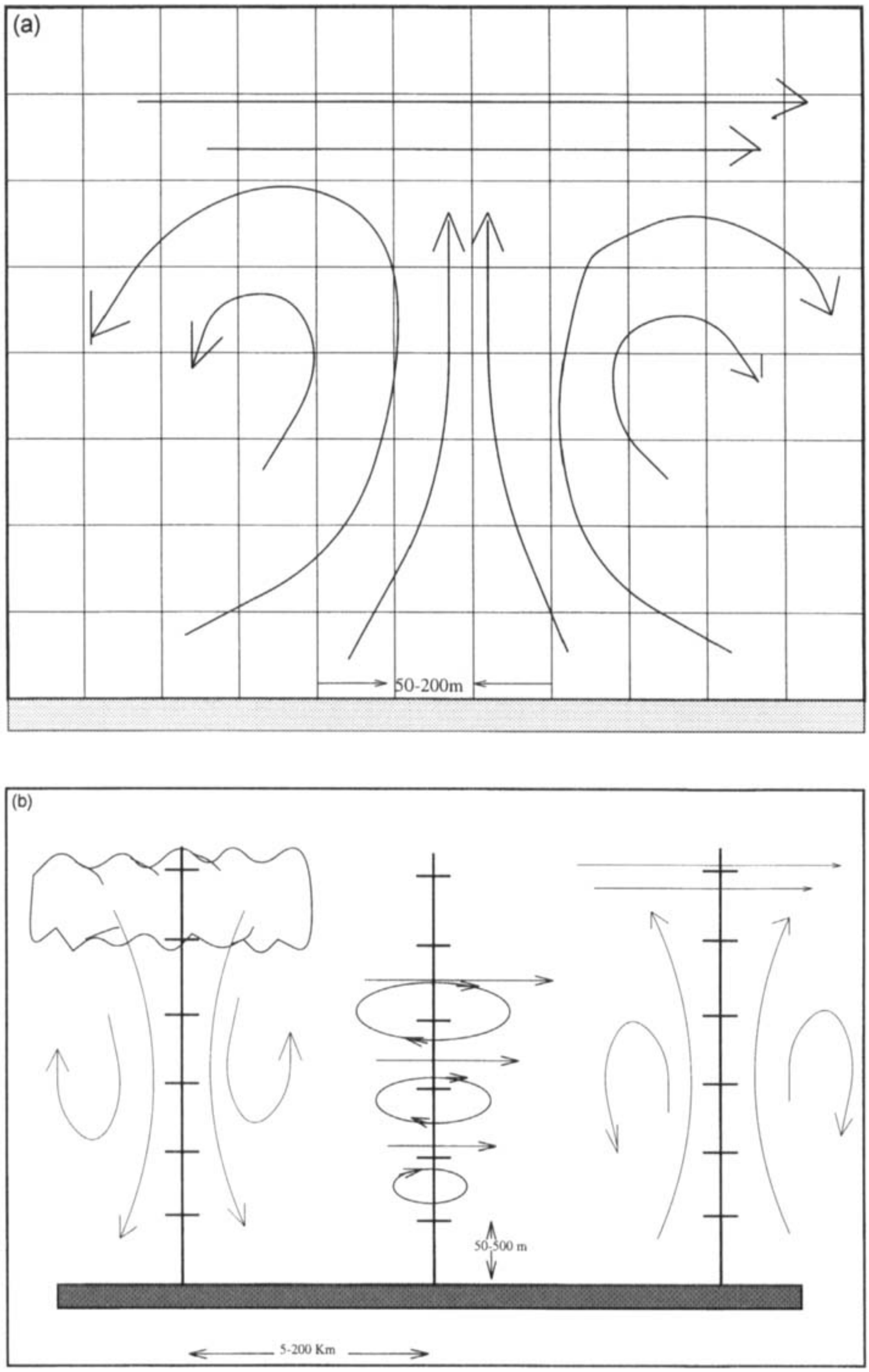

Figure 1. Schematic representation of boundary-layer motions in (a) a large-eddy simulation domain and (b) a mesoscale domain.

ensemble-type models (Sullivan *et al.* 1994). The correct representation of subgrid-scale motions in these cases is still an open research problem.

(ii) The representation of the turbulent motions, within mesoscale or general-circulation models, where the horizontal resolution precludes any attempt to resolve the turbulent motions but the vertical resolution is sufficient to build parametrizations accurate enough in various planetary boundary layer (PBL) configurations. Adjacent columns can represent very different flow regimes and are treated independently (Fig. 1(b)). The traditional approach has been to prescribe expressions for the vertical fluxes based on the analogy with the diffusion equation (e.g. Louis 1979; Holtslag and Boville 1993). A prognostic computation of the turbulent kinetic energy in limited-area models (LAMs) or general-circulation models (GCMs) is still not widely used because of computing limitations. The benefits of using a prognostic TKE have, however, been demonstrated in numerous papers (e.g. Mellor and Yamada 1974, 1982; Théry and Lacarrère 1983; Bougeault and Lacarrère 1989; Cuxart *et al.* 1994).

The Meso-NH model (Lafore *et al.* 1996) has been developed with regard to both large-eddy and mesoscale simulations, and we have elected to develop a single turbulence scheme for both configurations. This scheme is presented in section 2. It is based on earlier proposals by Redelsperger and Sommeria (1981,1986, hereafter RS81), and is generalized to include anelastic equations, sloping terrain and cloud processes. It is a complete three-dimensional SGS scheme, that comes from the second-order equation system for the turbulent moments, with a prognostic equation for the TKE and stability dependence functions derived from this equation system. It has been adapted to run also in single-column mode using the non-local mixing length of Bougeault and Lacarrère (1989) (hereafter BL89). The mixing-length expression is the only parameter of the scheme that varies from the LES to the mesoscale configuration. In particular, a single set of numerical closure constants is used for both configurations. The scheme is written in variables conserved during condensation and evaporation processes, to allow an easy treatment of non-precipitating cloud processes. In the present paper, however, we only report on the validation in dry mode.

In section 3, we report on three 'classical' LES-type simulations and compare our results with existing literature. Single-column experiments are shown in section 4. They are performed with the same numerical closure constants as the LES experiments, and behave satisfactorily. A comparison of mixing lengths as parametrized and estimated from spectral analysis of LES is also presented.

2. THE PROPOSED TURBULENCE SCHEME

(*a*) *Configuration of the scheme for LES*

The basis of the proposed turbulence scheme is the complete equation system for the second-order turbulent fluxes, variances and covariances. The reader is referred to Lilly (1967), Deardorff (1973) or Cuxart (1997) for the expanded set of equations, not written here for economy. This complete set of equations is too expensive computationally for the needs of LES and mesoscale simulations. It is necessary to drastically reduce its size, while keeping its physical significance if possible.

Following RS81, we retain only the full prognostic equation for the TKE, which represents the isotropic part of the Reynolds tensor. This equation provides a memory of the turbulence in the previous time-step. Furthermore, it allows the thermal stratification to be taken into account in the determination of the momentum fluxes in a simple way (through their dependence on the TKE). Finally, it allows a significant part of the turbulent transport to be represented. The equation reads

$$\frac{\partial e}{\partial t} = -\frac{1}{\rho_{\mathrm{ref}}}\frac{\partial}{\partial x_k}(\rho_{\mathrm{ref}}\overline{u_k}e) - \overline{u_i'u_k'}\frac{\partial \overline{u_i}}{\partial x_k} + \frac{g}{\theta_{\mathrm{v\,ref}}}\delta_{i3}\overline{u_i'\theta_{\mathrm{v}}'}$$

$$-\frac{1}{\rho_{\mathrm{ref}}}\frac{\partial}{\partial x_j}\left(-C_e\rho_{\mathrm{ref}}Le^{1/2}\frac{\partial e}{\partial x_j}\right) - C_\epsilon\frac{e^{3/2}}{L}. \tag{1}$$

It uses classical formulations for the dissipation and turbulent-transport terms. Here (u, v, w) are the velocities in the (x, y, z) direction, primes denote turbulent components, u_i and θ_{v} are the i-component of the velocity and the virtual potential temperature, while $\theta_{\mathrm{v\,ref}}$ and ρ_{ref} are the reference temperature and density profiles respectively and are specified once and for all. L is the mixing length, g is the acceleration due to gravity, $\delta_{i,j}$ is the Kronecker delta tensor and C_e and C_ϵ are closure constants.

For all other quantities such as fluxes and the anisotropic part of the Reynolds tensor, a simplified system of equations is derived, following the hypotheses of Sommeria (1976):

- The subgrid-scale turbulence is in stationary equilibrium with the boundary conditions on the grid cell, therefore the advection and time derivative terms are neglected.
- The external sources (radiative exchanges and large-scale effects) are neglected, which is equivalent to assuming a homogeneous spatial distribution of the sources into each grid cell.
- The dissipation by viscosity is neglected for fluxes and stresses, but not for the variances and scalar correlations.
- The Coriolis terms are neglected at these spatial scales.
- The third-order moments are neglected.
- Any anisotropic forcing is negligible compared to its isotropic counterpart when the latter is present in the equation.
- The spatial derivatives of the pressure-fluctuation terms are neglected
- The buoyancy terms are neglected in the equations for the anisotropic part of the Reynolds stresses but are conserved in the equations for isotropic momentum fluxes, and for the fluxes of heat, moisture or any other scalar.

The resulting system can then be solved analytically. This leads to the following expressions, which summarize our scheme:

$$\overline{u_i'u_j'} = \frac{2}{3}\delta_{ij}\, e - \frac{4}{15}\frac{L}{C_{\mathrm{m}}}e^{1/2}\left(\frac{\partial \overline{u_i}}{\partial x_j} + \frac{\partial \overline{u_j}}{\partial x_i} - \frac{2}{3}\delta_{ij}\frac{\partial \overline{u_m}}{\partial x_m}\right), \tag{2}$$

$$\overline{u_i'\theta'} = -\frac{2}{3}\frac{L}{C_s}e^{1/2}\frac{\partial \overline{\theta}}{\partial x_i}\phi_i, \tag{3}$$

$$\overline{u_i'q'} = -\frac{2}{3}\frac{L}{C_h}e^{1/2}\frac{\partial \overline{q}}{\partial x_i}\psi_i, \tag{4}$$

$$\overline{\theta'q'} = \frac{2}{3}\frac{1}{C_s}\frac{L^2}{C_{q\theta}}\left(\frac{\partial \overline{\theta}}{\partial x_m}\frac{\partial \overline{q}}{\partial x_m}\right)(\phi_m + \psi_m), \tag{5}$$

$$\overline{\theta'^2} = \frac{2}{3}\frac{1}{C_s}\frac{L^2}{C_\theta}\left(\frac{\partial \overline{\theta}}{\partial x_m}\frac{\partial \overline{\theta}}{\partial x_m}\right)\phi_m, \tag{6}$$

$$\overline{q'^2} = \frac{2}{3}\frac{1}{C_h}\frac{L^2}{C_q}\left(\frac{\partial \overline{q}}{\partial x_m}\frac{\partial \overline{q}}{\partial x_m}\right)\psi_m, \tag{7}$$

$$\overline{u_i'\theta_v'} = -\frac{2}{3}\frac{L}{C_s}e^{1/2}\left(E_\theta\frac{\partial\overline{\theta}}{\partial x_i}\phi_i + E_q\frac{\partial\overline{q}}{\partial x_i}\psi_i\right), \tag{8}$$

$$\overline{u_i'S'} = -\frac{2}{3}\frac{L}{C_S}e^{1/2}\frac{\partial\overline{S}}{\partial x_i}\psi_{svi}. \tag{9}$$

Here p, q and S are the pressure, the specific humidity, and the concentration of any scalar quantity, respectively, and ϕ_i and ψ_i are stability functions. Subscripts s, h and svi stand for sensible heat, latent heat and the ith scalar variable, respectively, and the Einstein summation convention applies for subscripts m. Equivalent equations for the variance of scalars and correlation of scalars with θ and q can also be written, introducing new constants (C_S, $C_{S\theta}$, C_{Sq}). The virtual potential temperature is linked to temperature and humidity by the coefficients $E_\theta = \overline{\theta_v}/\overline{\theta}$, and $E_q = 0.61\overline{\theta}$. Note that these factors have more complex expressions when phase changes are present. The present paper does not address these aspects but the interested reader will find the complete expressions in RS81.

The numerical constants appearing in the above equations originate from the closure terms: the primary closure constants C_m, C_s, C_h, C_S come from the pressure-correlation parametrization, while C_θ, C_q, $C_{q\theta}$ and C_ϵ come from the dissipation parametrization. C_e is involved in the turbulent transport of TKE. For the present study, the same values as in RS81 are used: for the dry processes, $C_m = 4$, $C_s = C_m$, $C_\epsilon = 0.7$, $C_\theta = 1.2$; for the moist processes, $C_h = C_s$, $C_q = C_\theta$, $C_{q\theta} = 2C_\theta$. C_e is taken equal to 0.4, which proves to work fine both in LES and single-column modes. Alternative values had been proposed by Schmidt and Schumann (1989, hereafter SS89, appendix B). The largest difference between the values of RS81 and those of Schmidt and Schumann, is for C_ϵ taken equal to 0.845. The present choice is supported by the following arguments: first, Schmidt and Schumann work in dry conditions, and do not provide constants for moist processes, already tested by RS81; second, after performing some sensitivity tests, Krettenauer and Schumann (1992) using the same model changed the set of constants to values much closer to those of RS81. Note that contrary to the dry and moist processes, there is no previous record or theoretical support for the values of the numerical constants used in the equation for the scalar constituants. C_S is taken equal to the corresponding value for vapour, i.e. C_h, and $C_{S\theta} = C_{Sq} = C_{q\theta}$.

In expressions above, the quantities ϕ_i, ψ_i and ψ_{svi} are inverse turbulent Prandtl and Schmidt numbers, that can be computed from the initial equations without any additional assumption. The equations take the general form

$$\overline{u_i'\xi'} = -\frac{2}{3}\frac{1}{C_\xi}Le^{1/2}\frac{\partial\xi}{\partial x_i}\underbrace{\left\{1 - \delta_{i3}\frac{g}{\theta_{\mathrm{v\,ref}}}\frac{\overline{\theta_v'\xi'}}{e(\partial\xi/\partial x_i)}\right\}}_{f_i} \tag{10}$$

for $\xi = \theta, q, S$ and $f_i = \phi_i, \psi_i, \psi_{svi}$. Thus, ϕ_i, ψ_i and ψ_{svi} are unity for $i = 1, 2$, and their value for $i = 3$ depends on e and the 3D local variations of the fields and casts the buoyancy effects $\overline{\theta_v'\xi'}$ into the expressions for the fluxes. This reads

$$\phi_3 = 1 - \frac{(1 + C_1R_q)(2C_2R_{q\theta}^2 + C_1R_\theta^{*2})(1/(R_\theta) + C_1C_2(R_\theta^{*2} - R_q^{*2})}{1 + (C_1 + C_2)(R_\theta + R_q) + C_1\{C_2(R_\theta^2 + R_q^2) + C_1R_\theta R_q\}}, \tag{11}$$

$$\psi_3 = \psi(R_\theta, R_\theta^*, R_q, R_q^*, R_{q\theta}) = \phi(R_q, R_q^*, R_\theta, R_\theta^*, R_{q\theta}), \tag{12}$$

$$\psi_{sv3} = \frac{1 - \frac{2}{3}\left[\frac{1}{R_S}\{C_a(R^2_{S\theta} - R_\theta R_S) + C_b(R^2_{Sq} - R_q R_S)\} + \frac{1}{C_S C_{S\theta}} R_\theta \phi_3 + \frac{1}{C_S C_{Sq}} R_q \psi_3\right]}{1 + \frac{2}{3}\frac{1}{C_{S\theta} C_S} R_\theta + \frac{2}{3}\frac{1}{C_{Sq} C_S} R_q}. \tag{13}$$

Some derived constants have been introduced:

$$C_1 = (2/3)(1/C_s C_\theta), \quad C_2 = (2/3)(1/C_s C_{q\theta}).$$

In the above equations, the R^* are generalized Richardson numbers introduced in RS81 and extended here for scalar quantities, and have the following definitions:

$$R_\theta = A E_\theta \frac{\partial \overline{\theta}}{\partial x_3}, \quad R_q = A E_q \frac{\partial \overline{q}}{\partial x_3}, \quad R_S = A \frac{\partial \overline{S}}{\partial x_3}, \tag{14}$$

$$R^*_\theta = A E_\theta \left(\frac{\partial \overline{\theta}}{\partial x_m} \frac{\partial \overline{\theta}}{\partial x_m}\right)^{1/2}, \quad R^*_q = A E_q \left(\frac{\partial \overline{q}}{\partial x_m} \frac{\partial \overline{q}}{\partial x_m}\right)^{1/2}, \tag{15}$$

$$R^2_{q\theta} = A^2 E_\theta \frac{\partial \overline{\theta}}{\partial x_m} E_q \frac{\partial \overline{q}}{\partial x_m}, \quad R^2_{S\theta} = A^2 E_\theta \frac{\partial \overline{S}}{\partial x_m} \frac{\partial \overline{\theta}}{\partial x_m}, \quad R^2_{Sq} = A^2 E_q \frac{\partial \overline{S}}{\partial x_m} \frac{\partial \overline{q}}{\partial x_m}, \tag{16}$$

with

$$A = \frac{g}{\theta_{\mathrm{v\,ref}}} \frac{L^2}{e}, \quad C_a = \frac{1}{C_{S\theta}}\left(\frac{1}{C_S} + \frac{1}{C_s}\right), \quad C_b = \frac{1}{C_{Sq}}\left(\frac{1}{C_S} + \frac{1}{C_h}\right). \tag{17}$$

The behaviour of these stability functions will be described later.

In order to close the above system, an expression is needed for the largest eddy length-scale L. This quantity appears from the parametrizations of the dissipation, turbulent transport and pressure correlation. It is assumed that a single expression is sufficient for the three processes. The length-scale represents the size of the largest energetic eddies feeding the cascade of energy down to dissipation. Its practical calculation should therefore rely on the determination of the largest subgrid eddy size at each grid point. For LES in the 3D framework, the largest unresolved eddies are by definition of the size of the grid cell, hence

$$L = (\Delta x \Delta y \Delta z)^{1/3}. \tag{18}$$

Note that this relies on the hypothesis that the grid size falls into the inertial subrange. This is clearly not true in the presence of strong stable stratification or near the ground, and in such regions a better phenomenological determination of the length-scale should be used. This will be considered in the future.

(*b*) *Configuration for mesoscale modelling*

When the scheme is used at the mesoscale (say, horizontal grid sizes larger than 2 km), it can be assumed that the horizontal gradients and turbulent fluxes are much smaller than their vertical counterparts. Therefore only the vertical computations need to be done. This is recognized in the organization of the computer code, which performs the computations of the vertical gradients and fluxes in separate subroutines. Furthermore the temporal integration scheme is a semi-implicit Crank–Nicholson for the vertical part, allowing for large time-steps, while it is explicit for the horizontal part in the LES configuration.

The validity of the hypotheses above at the mesoscale should be seriously questioned. Probably it is less justified to neglect the third-order moments, as vertical transports can be quite significant in convective situations (e.g. Canuto *et al.* 1994; Cuijpers and Holtslag 1998). However, for sake of simplicity, we have decided to keep the same hypotheses. Let us recall here that turbulent transports are only neglected in the equation for the anisotropic part of the Reynolds tensor, and that the turbulent transport is fully retained in the TKE prognostic equation.

In the mesoscale configuration, the expressions of ϕ_3, ψ_3 and ψ_{sv3} retain only the vertical gradients, leading to $R_\theta^* = R_\theta$, $R_q^* = R_q$, $R_{q\theta}^2 = R_q R_\theta$, $R_{S\theta}^2 = R_S R_\theta$ and $R_{Sq} = R_S R_q$. Thus,

$$\phi_3 = \psi_3 = \psi_{sv3} = \frac{1}{1 + C_1 R_{1\mathrm{D}}}, \tag{19}$$

with

$$\begin{aligned} R_{1\mathrm{D}} &= (R_\theta + R_q) \\ &= \frac{g}{\theta_{\mathrm{v\,ref}}} \frac{L^2}{e} \left(E_\theta \frac{\partial \overline{\theta}}{\partial z} + E_q \frac{\partial \overline{q}}{\partial z} \right) \\ &= \frac{g}{\theta_{\mathrm{v\,ref}}} \frac{L^2}{e} \frac{\partial \overline{\theta_{\mathrm{v}}}}{\partial z}. \end{aligned} \tag{20}$$

To get insight into the physical behaviour of stability functions, it is useful to derive approximated expressions. Assuming a stationary equilibrium of TKE and neglecting its turbulent transport, ϕ_3 can be approximated as:

$$\phi_3 \simeq \frac{1}{1 + C_4 Ri / f(Ri)}, \tag{21}$$

$$f(Ri) = 0.5\{1 - (C_3 + C_4) Ri + [\{1 - (C_3 + C_4) Ri\}^2 + 4 C_4 Ri]^{1/2}\}, \tag{22}$$

where Ri is the usual Richardson number and $C_3 = 5C_\mathrm{m}/2C_s$, $C_4 = 5C_\mathrm{m}C_\epsilon/2C_sC_\theta$.

This expression is plotted in Fig. 2(a). Note that the approximated ϕ_3 is unity when the Richardson number is zero (no stability effect), goes to large values for negative *Ri*, and to small values for positive *Ri*. The different mixing efficiency of momentum, heat or scalars has been a subject of study for some forty years. Here the stability functions allow the scheme to have very different turbulent-exchange coefficients for some stability conditions, as suggested by laboratory experiments (e.g. Arya 1972), field campaigns (e.g. Yagüe and Cano 1994) and numerical simulation (Brost and Wyngaard 1978; Holtslag and Moeng 1991). Theoretical arguments can also be found in Schumann (1991) for stably stratified layers, supporting the idea that the mixing efficiency for momentum must be larger than for heat in order to sustain the wind shear. The behaviour of approximated ϕ_3 shown in Fig. 2(a) is consistent with the proposals found in the above mentioned literature.

The full expression for ϕ_3 (tridimensional and with phase changes) follows the same behaviour qualitatively, though it is more difficult to make a simplified analysis from the equations. For small unstable gradients, such as $|C_1(gL^2/\theta_{\mathrm{v\,ref}})(\partial\theta/\partial z)| < |e|$, ϕ_3 becomes bigger than 1, enhancing mixing, but when $|C_1(gL^2/\theta_{\mathrm{v\,ref}})(\partial\theta/\partial z)| > |e|$ (very unstable stratification) then ϕ_3 becomes negative, with a singularity separating both regimes. This is an artefact due to the over-simplification of the initial equations. To avoid the singularity, the value of the stability functions has been limited by a threshold

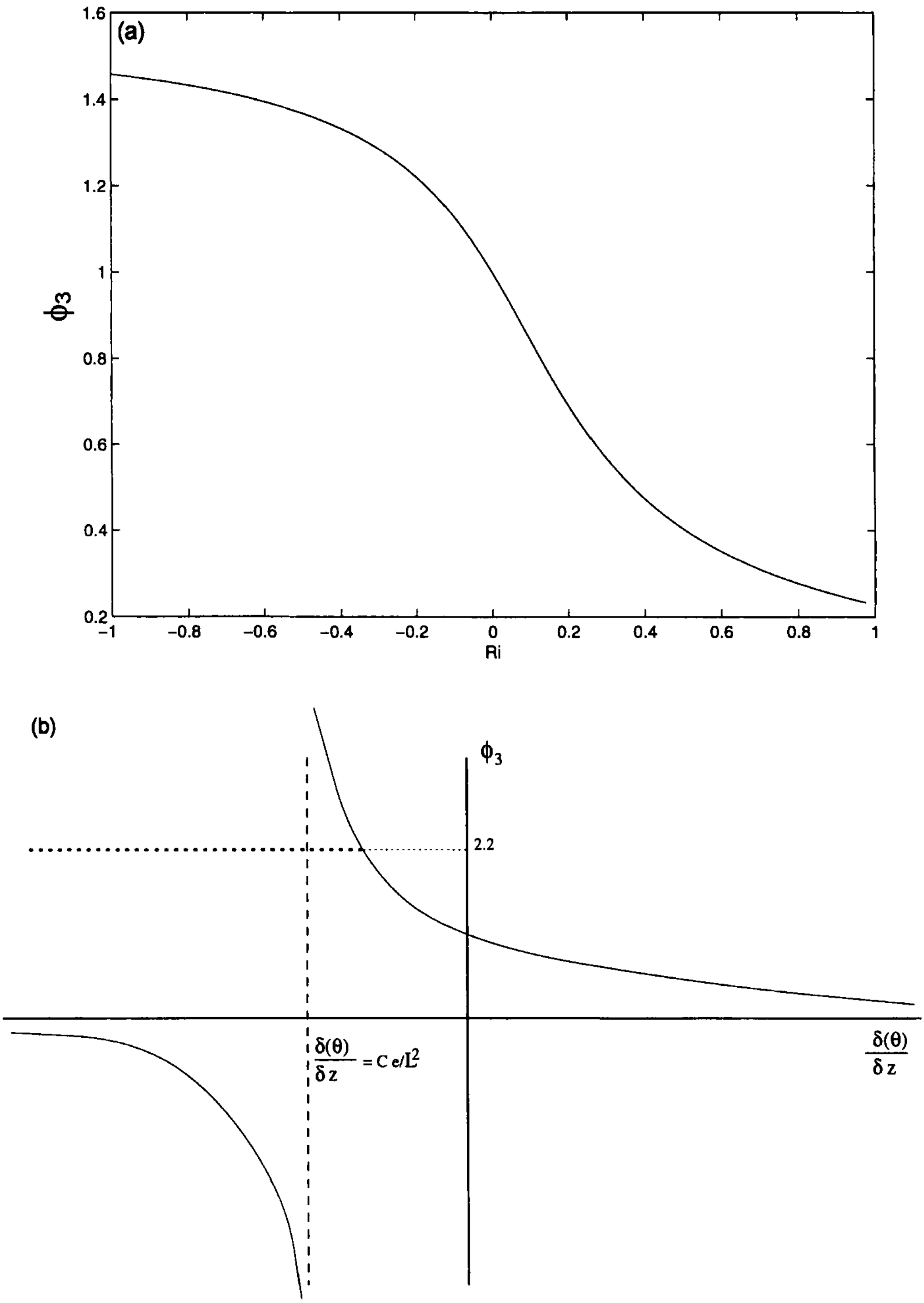

Figure 2. Behaviour of the 1D dry ϕ_3 function as function of (a) Richardson number (approximate function) and (b) generalized Richardson number R_θ. See text for explanation of symbols.

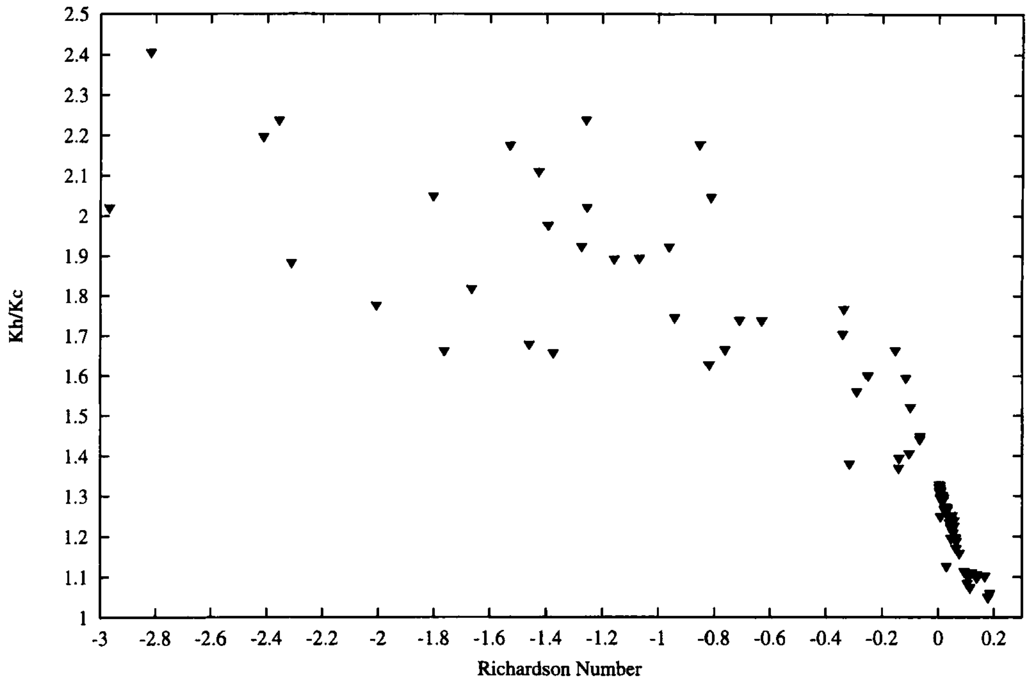

Figure 3. Measured values of the inverse turbulent Prandtl number (from Yagüe and Cano (1994)).

value of 2.2 (Fig. 2(b)). This is justified by two independent arguments. First, when the scheme is applied with very small time-steps, the singularity condition is never reached because the unstable temperature gradient never takes large values. In these conditions, the maximum value of ϕ_3 is found to lie between 2.0 and 2.2. Secondly, observations in the surface layer from Yagüe and Cano (1994) show a value of the inverse Prandtl number ranging between 1.6 and 2.2 in unstable conditions (Fig. 3). Unfortunately, the use of a threshold value prevents ϕ_3 and ψ_3 from becoming negative and does not allow the scheme to have counter-gradient behaviour, even though the derived formula formally includes this effect. Indeed, expanding (10) for $\xi = \theta$ in dry mode ($\theta_v = \theta$) leads to

$$\overline{w'\theta'} = -\frac{2}{3}\frac{1}{C_h} L e^{1/2} \left(\frac{\partial \overline{\theta}}{\partial z} - \frac{g}{\theta_{\text{ref}}} \frac{\overline{\theta'^2}}{e} \right) \tag{23}$$

that closely parallels the Deardorff (1972b) expression for the counter-gradient: $\gamma_c = \overline{\theta'^2}/e$ instead of $\gamma_c = \overline{\theta'^2}/\overline{w'^2}$ in Deardorff's proposal. Nevertheless, this advantage is partly lost in the resolution of the equation, leading to (19).

In the mesoscale framework, all 3D turbulent motions are subgrid, but the higher vertical resolution should allow the size of the most energetic eddies to be parametrized in a physical way at every level. This can be done through the length-scale specification, which is the only free parameter. A classical approach has been to use the Blackadar mixing length, where asymptotic behaviours are forced through an adjustable parameter. This formulation is case-dependent and introduces a large arbitrariness in the choice of the parameter. Another approach in atmospheric modelling is the $e - \epsilon$ model, where the length-scale is implicitly obtained by means of a prognostic equation for the dissipation of turbulent kinetic energy. This approach is very attractive, since it circumvents the need

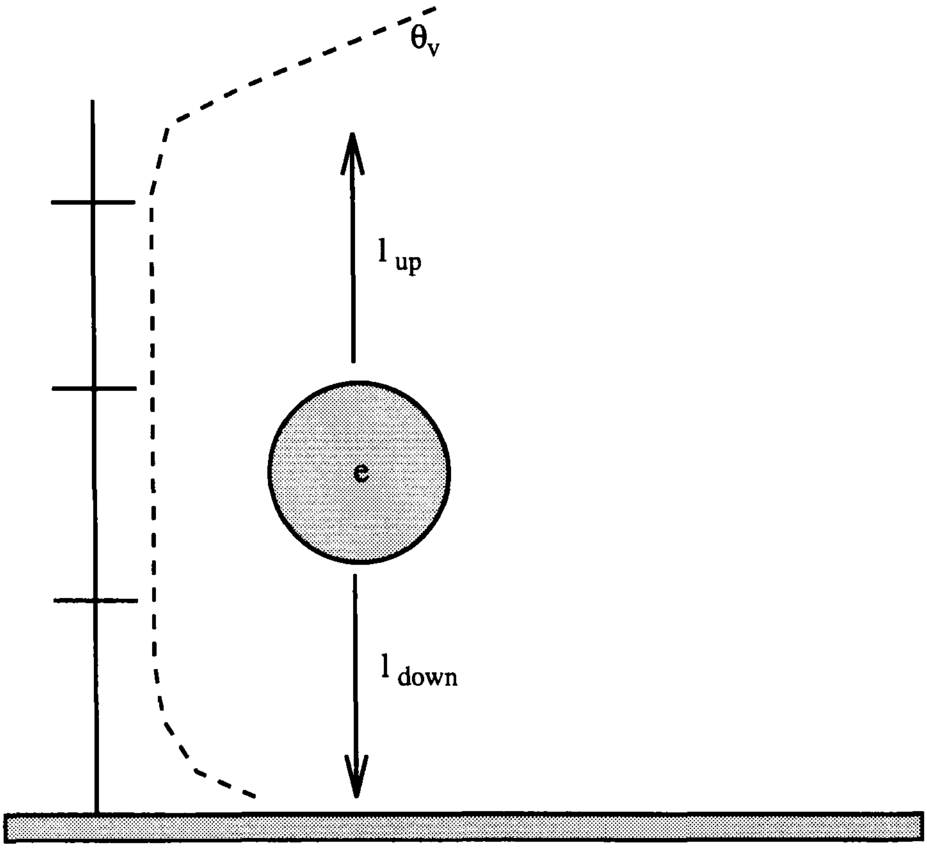

Figure 4. Schematic view of the Bougeault–Lacarrère length for a convective boundary layer. See text for explanation.

for a parametrization of the length-scale, but then the problem is moved to the handling of the dissipation equation, which is very difficult in the presence of stratification.

In the present scheme the length-scale formulation of Bougeault and Lacarrère (BL89) is used because it seems physically well founded. The length-scale of the largest eddies at a given level is determined as a function of the stability profile of the adjacent levels. The algorithm relies on the computation of the maximum vertical displacement allowed, for a parcel of air having the mean kinetic energy of the level as initial kinetic energy. The maximum upward displacement is called l_{up} and the maximum downward displacement is called l_{down}. These quantities are computed by assuming that the parcel will stop when the cumulated buoyancy accelerations equal the initial kinetic energy (Fig. 4):

$$\int_{z}^{z+l_{\mathrm{up}}} \frac{g}{\theta_{\mathrm{v\,ref}}}(\theta_{\mathrm{v}}(z') - \theta_{\mathrm{v}}(z))\,\mathrm{d}z' = e(z),$$
$$\int_{z-l_{\mathrm{down}}}^{z} \frac{g}{\theta_{\mathrm{v\,ref}}}(\theta_{\mathrm{v}}(z) - \theta_{\mathrm{v}}(z'))\,\mathrm{d}z' = e(z). \tag{24}$$

Then $L = (l_{\mathrm{up}} l_{\mathrm{down}})^{1/2}$. This method allows the length-scale at any level to be affected not only by the stability at this level, but by the effect of remote stable zones ('non-local' length). In the present scheme, a second-order accuracy algorithm has been implemented to evaluate $l_{\rm up}$ and $l_{\rm down}$ from (24). With this method, the evaluation of $l_{\rm up}$ and $l_{\rm down}$ in uniformly stratified layers supplies the well-known expression for the length-scale proposed by Deardorff (1980):

$$L = \left\{ \frac{2e}{(g/\theta_{\rm v\,ref})(\partial\theta_{\rm v}/\partial z)} \right\}^{1/2}. \tag{25}$$

This is an interesting feature of the scheme, which can be seen as a non-local generalization of previous approaches.

At the present time, the length-scale algorithm does not allow for the effects of lateral entrainment into the rising parcel. This is probably not important for stably stratified layers, and it will be shown later that the length-scale computed in dry convective boundary layers by the present algorithm is satisfactory. The problem could become significant in moist convective situations, especially for boundary-layer cumulus clouds. This is a subject for further improvement of the scheme when it will be applied for cloudy boundary layers. The limitations of the present algorithm may be removed in the future thanks to extensive use of LES outputs as discussed later.

Usually subgrid-scale (for LES) and single-column turbulence schemes (for LAMs or GCMs) use different sets of constants. This is often considered as unavoidable, as the range of scales represented in these two types of model—and therefore their spectral behaviour—are quite different. In the present case, the same set of constants is used for both the SGS and the single-column formulations. The use of the ϕ_3 stability function is a key element for this generality. If ϕ_3 is set to unity, as in some more simple turbulence models, it is impossible to use a single set of numerical constants for all applications. This is a strong argument in favour of the present proposal.

Assuming stationary equilibrium for TKE and neglecting the turbulent transport, the TKE equation reads:

$$\begin{aligned}\frac{\partial e}{\partial t} &\simeq 0\\ &\simeq \frac{4}{15C_{\rm m}} L e^{1/2}\left(\frac{\partial \overline{u}}{\partial z}\right)^2 - \frac{g}{\theta_{\rm v\,ref}}\frac{2}{3C_s} L e^{1/2}\frac{\partial\overline{\theta_{\rm v}}}{\partial z}\left(1 + C_1\frac{L^2}{e}\frac{g}{\theta_{\rm v\,ref}}\frac{\partial\overline{\theta_{\rm v}}}{\partial z}\right)^{-1} - C_\epsilon\frac{e^{3/2}}{L}.\end{aligned} \tag{26}$$

With these approximations in the single-column model configuration, using the expression of the mixing length for stable stratification, a critical Richardson number can then be obtained:

$$Ri_{\rm c} = \frac{N^2}{\left(\dfrac{\partial u}{\partial z}\right)^2} = \frac{(4\sqrt{2}/15C_{\rm m})}{\dfrac{2\sqrt{2}}{3C_s}\left(\dfrac{1}{1+2C_1}\right) + \dfrac{C_\epsilon}{\sqrt{2}}}. \tag{27}$$

With the RS81 values for the numerical constants, $Ri_{\rm c} \simeq 0.139$. This is admittedly a low value, though it has been obtained for very restrictive conditions. Another choice for the numerical constants could lead to some higher value of the critical Richardson number.

Finally, we should note that with the formulation (25) of L under uniform stable stratification, the value for ϕ_3 is nearly constant and equal to $(1 + C_1)^{-1} = 0.78$. On the other hand, at interfaces between stable and unstable layers, such as the inversion at the top of a convective layer, the factor L^2/e in ϕ_3 behaves in a different manner from when it is inside a pure stable or unstable layer. Just below the inversion, L can be quite large, as downdraughts are originating from that layer. Meanwhile, e has moderate value, and the factor L^2/e becomes rather large, leading to values of ϕ_3 much smaller than 0.78. So, the scheme will strongly inhibit mixing through a stability interface while allowing some mixing inside a more uniformly stratified layer.

3. Validation in LES mode

Three paradigmatic regimes of the PBL (convective, shear driven and dry emulation of a stratocumulus) have been simulated to validate our new model. A complete description of the results is given by Cuxart (1997). Let us stress again that all simulations have been made with the same set of constants and the same closure for the mixing length.

(*a*) *Convective boundary layer*

A simplified case of a dry convective boundary layer with no mean wind was proposed (Nieuwstadt *et al.* 1993) to intercompare the results of four different LES codes. The original set-up of Schmidt and Schumann (1989) was taken on the same domain $(L_x, L_y, L_z) = (6400, 6400, 2400)$ m, but instead of a resolution of $(50\ \text{m})^3$ a smaller number of points (40^3) was used leading to $\Delta x = \Delta y = 160$ m, $\Delta z = 60$ m. In order to minimize the factors leading to differences, zero mean wind and dry conditions are imposed, with constant surface heating and roughness prescribed. After a three-hour run, the statistics are computed on the last 20 minutes. A high-resolution run was also made, with the same characteristics as the SS89 simulation.

Our model is able to reproduce the main features of such a PBL, both for the standard and the high-resolution runs, with a well-mixed layer under an undulating inversion. For economy purposes, only a few figures will be shown here. The reader is referred to Cuxart (1997) for a more extensive comparison. The updraughts form in the surface layer quite randomly and, at a height of one-third of the PBL, they form some narrow columns that may reach the inversion, performing much of the transport of the surface-layer air. These updraughts deform the inversion and produce locally unstable stratification, generating entrainment of the upper stable layer into the mixed layer. Slower and wider downdraughts form by continuity. The cells generate low-level winds, with zero mean value, but enhance the turbulence production through friction.

A comparison of the time- and space-averaged heat fluxes from the standard-resolution run (SR) and the high-resolution run (HR) with four reference models is shown for the total and the subgrid part on Figs. 5(a) and 5(b), respectively. In the SR run, the entrainment at the top of the convective layer is found to be somewhat larger than for the reference models. This was found to be due to the effect of the ϕ_3 function, that enhances the mixing at the sides of the impinging updraughts. However, the computed value for the SR run of $-0.23Q_s$ (Q_s being the value of the surface flux) lies in the range of observed experimental values(from zero to $-0.4Q_s$). It must be noted that the HR run entrains less, showing a sensitivity to resolution much larger than changes in the SGS scheme. SS89 use a modified mixing length for the subgrid heat flux and obtain the highest entrainment rate of the four reference models, indicating the same behaviour as in our model. As expected, the averaged SGS contribution to the total flux is small everywhere except near the ground and at the inversion (Figs. 5(b) and 13(b)). The averaged ϕ_3 function is shown in Fig. 6(a) for both resolutions. Despite local high values of ϕ_3 at impinging updraughts, the averaged value at the inversion is small. This averaged quantity is an indicator of the stability of a given layer. A change in the averaged value of ϕ_3 with resolution is observed in the interior of the mixed layer,

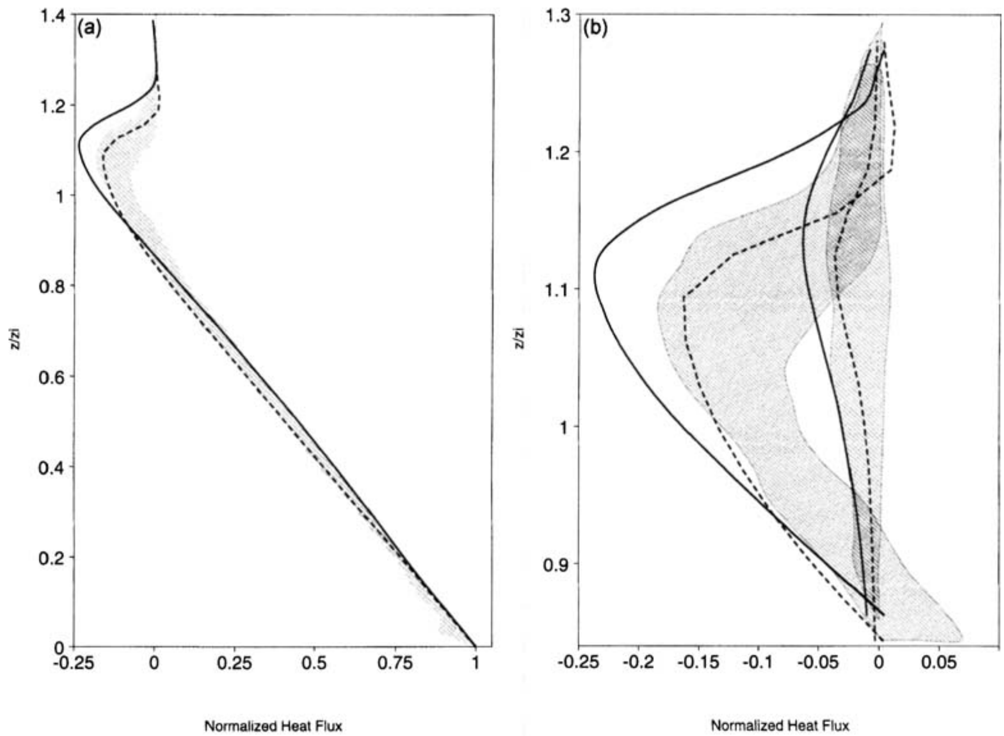

Figure 5. Comparison of vertical heat flux in large-eddy simulation mode for the convective boundary-layer case against data and four other models: (a) total and (b) total and subgrid parts in the entrainment zone. Solid line—standard-resolution run, dashed line—high-resolution run, shaded areas—ensemble of four intercompared models. z/z_i is height normalized by boundary-layer height.

with the HR run being neutrally stratified except near the ground and at the inversion layer, while for SR unstable stratification is shown in the lower third of the mixed layer and stable stratification above that height.

In Fig. 7, the spectra of the u component of the wind at three different levels of SR and HR runs is plotted against the ensemble of three models, with the dotted line representing the UK Meteorological Office Model (UKMO) backscatter run that behaves very differently at high wave numbers. The spectra fall in the range of the three intercompared models, with a departure from the $-5/3$ slope at the highest wave numbers due to the low horizontal resolution. On the other hand, the HR run reproduces a good inertial subrange at the three levels. This is an indication of the good quality of the HR run.

A new diagnostic has been obtained from the time and space averages of spectra at every level. The detection of the most energetic mode at every level is used to obtain the scale of this mode, dividing the length of the domain by the mode number. The isotropy of this simulation allows spectral computations in the x direction to be performed without losing generality. A vertical profile of the most energetic scales is obtained for each analysed variable. This will be called the 'spectral length' (SL) hereafter.

Spectral lengths are an interesting tool for interpreting LES statistics, with a possible application to improve the parametrization of the mixing lengths in mesoscale models. SL for u, v, w and e are shown in Fig. 8. The SL of u show maxima near the ground and at the inversion layer, with values of 3200 m, that correspond to half the size of horizontal domain. A minimum is obtained in the interior of the mixed layer, with a

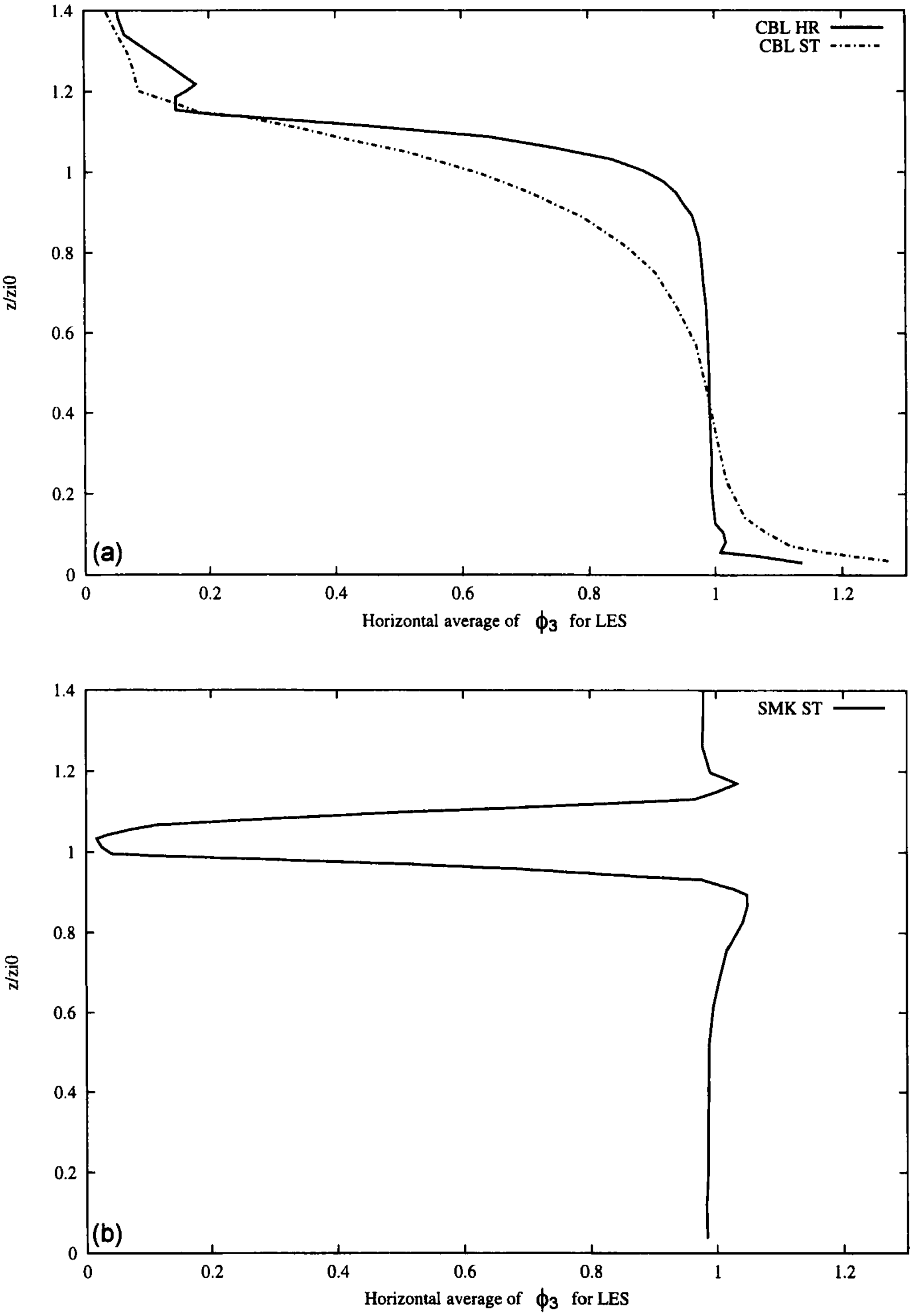

Figure 6. Averaged stability function ϕ_3 in large-eddy simulation mode for (a) the convective boundary-layer case (solid line—high resolution run, dashed line—standard resolution run) and (b) the smoke-cloud case. z/z_{i0} is the height normalized by the initial boundary-layer height.

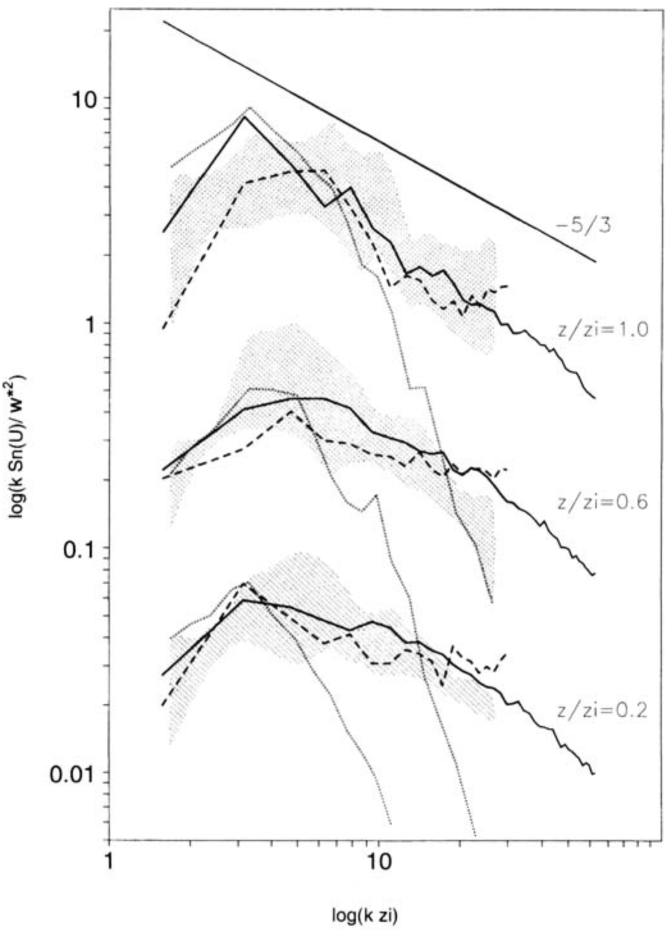

Figure 7. Normalized spectra of horizontal velocity u at the standard horizontal resolution (160 m)—dashed, and high resolution (50 m)—solid, for the convective boundary-layer case at three heights compared to three models (shaded area) and the backscatter run of Mason and Brown (dotted line). k is wave number, z_i is boundary-layer height and w^* is the convective velocity.

value close to the size of the thermals. The same qualitative behaviour is observed for v. However, the SL for w has minima near the ground and the inversion layer, and a maximum in the middle of the mixed layer. This behaviour is consistent with the inspection of the 3D fields (not shown). Both horizontal boundaries (the ground and the inversion) act as lids forcing horizontal circulations. The maximum of w is located at the height where the largest number of shallow thermals is found. The field indicates a quasi-isotropic behaviour in the mixed layer and a strongly anisotropic behaviour near its boundaries. Indeed, corresponding to the circulations created by the wall effect, the size of the w structures is strongly reduced, whereas the u component is stretched.

The intercomparison shows that the SGS contribution is somewhat larger near the ground than for the other models. This may be related to our treatment of the shear production at the first computation point (extrapolation of the lowest gradient of wind). Nevertheless, the normalized value of $\langle w'^2 \rangle$ at the ground is smaller than $1.8(z/z_i)^{2/3}$, where z_i is the height of the boundary layer, which is the currently admitted maximum value from observation.

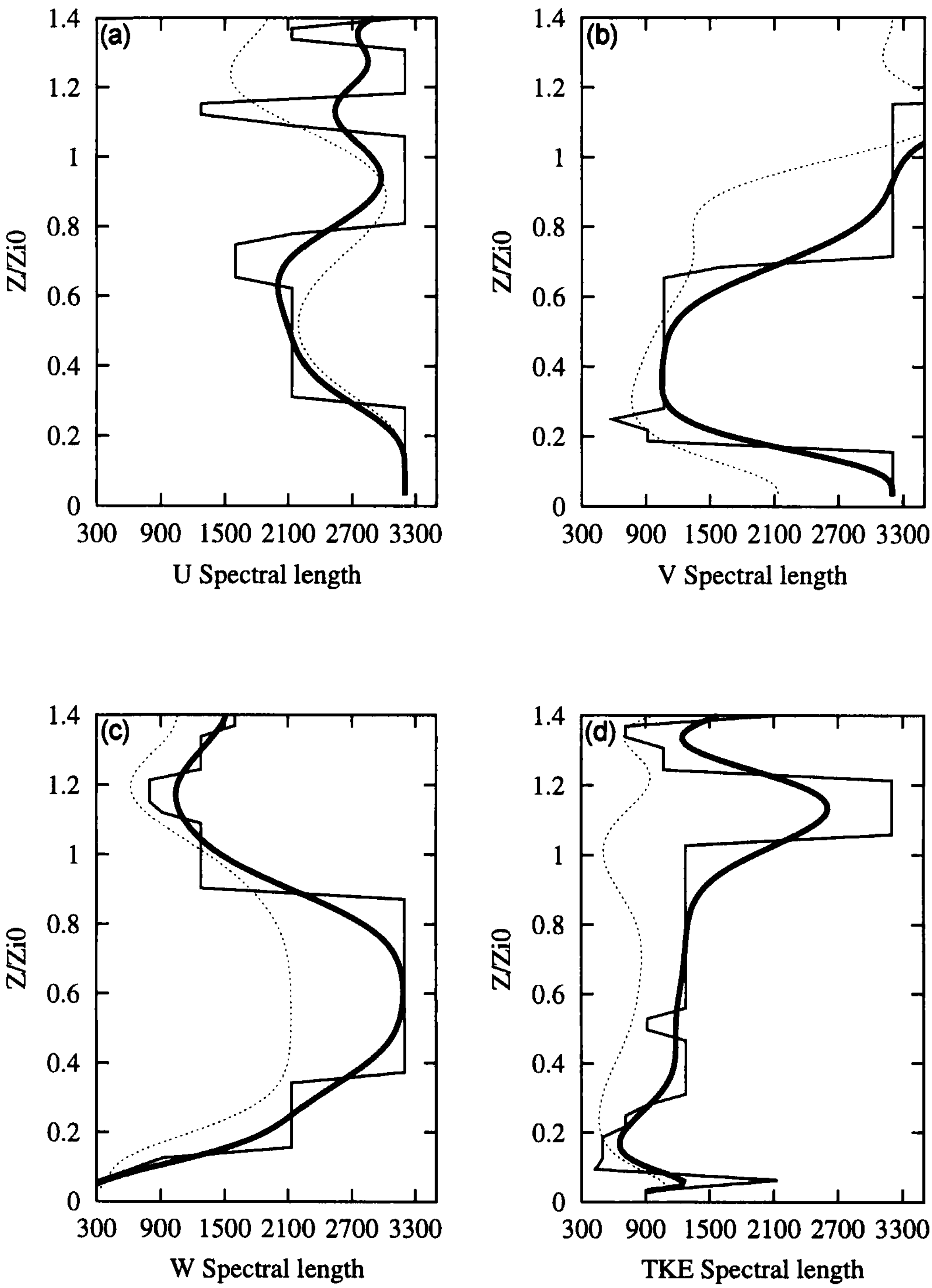

Figure 8. Vertical profiles of spectral lengths (m) of velocity components (a) u, (b) v and (c) w, and (d) resolved turbulent kinetic energy for the convective boundary-layer case. Solid line—non-smoothed high-resolution (HR) outputs, thick solid lines—smoothed HR outputs, dotted line—smoothed standard-resolution outputs. z/z_{i0} is height normalized by the initial boundary-layer height.

The resolved kinetic energy is mainly generated by buoyant processes and the subgrid kinetic energy by local shear on the sides of the updraughts and by friction near the ground. At the inversion we may note local maxima for the SL of the resolved kinetic energy, which may be related to trapped waves (Fig. 8(d)).

(*b*) *Smoke-cloud case*

The turbulent structure of the cloud-topped PBL is complex because of the important role played by radiative fluxes and water phase changes, together with evaporative cooling, entrainment of warm and dry air from above the cloud, large-scale divergence and turbulent buoyancy fluxes. LES models are considered a promising tool for understanding the role of the these processes, but their ability to deal with such complex processes needs to be assessed. A first step is to examine the entrainment rates of LES models in a simple case of a smoke cloud, i.e. without any phase change. It was the object of an intercomparison of LES models including the present one (Bretherton *et al.* 1999). For this case, an initial uniform concentration of a radiatively active smoke tracer is imposed below the inversion. The radiative cooling is imposed as a function of the scalar concentration, and only in the smoke layer, similar to what is observed in stratocumulus clouds. A three-hour run is performed on a domain of $L_x = L_y = 3200$ m, $L_z = 1250$ m with horizontal and vertical resolutions of 50 m and 25 m respectively. The statistics are performed over the last hour. Free slip, rigid-lid top and bottom boundary conditions are prescribed, with no surface fluxes. A well-mixed constant potential-temperature profile is imposed as initial conditions under a 7 K inversion at 700 m. A zero-mean wind profile is chosen, with no subsidence or Coriolis forcing, and a roughness length of 0.1.

The mixed layer deepens about 40 m during the three-hour run, meaning that entrainment occurs during the simulation. Vertical cross-sections under the inversion of θ and w (not shown) show narrow cold plumes originating at the inversion and falling to the ground. The plumes are separated by distances around 1600 m, and their vertical dimension is approximately equal to the height of the layer under the inversion (about 650 m). The averaged stability function ϕ_3 is almost everywhere close to 1 in the mixed layer. However, the region below the inversion, where downdraughts form, has some very unstable stratification with large values of ϕ_3 (Fig. 6(b)). The heat-flux profile is very close to the currently accepted value for stratocumulus, and compares well with the results of the other models (Fig. 9). The subgrid-scale contribution is very small in the lower layer, but explains much of the flux at the inversion (Fig. 15(b)). This can be attributed to the stability function ϕ_3 that shows a very *small mean* value at the inversion, but exhibits *strong local* values at that level enhancing the mixing at the sides of the downdraughts. The results are very sensitive to the subgrid-scale scheme at that level, because the grid size is much larger than the largest eddies. Several of the reference models used the Smagorinsky (1963) subgrid scheme, together with the Deardorff length-scale. Their results are therefore close to each other.

The spectra show that, at the present resolution, an inertial subrange is generated in the mixed layer, but it is not following the $-5/3$ slope at the inversion layer. The SL for u, v, w and e are plotted in Fig. 10. As for the previous case, the same conclusion can be reached from the inspection of the 3D fields (not shown) and from the SLs. The horizontal velocity variances show maxima under the inversion (generation of the downdraughts and horizontal motions generated by continuity) and near the ground. The w variance has a maximum at the middle of the boundary layer, where the plumes are best defined. The same behaviour is observed on the SL plots (Fig. 10). The skewness presents a negative peak value under the inversion, supported by the observations and that only a few LES models are able to capture. The spectral length for the resolved

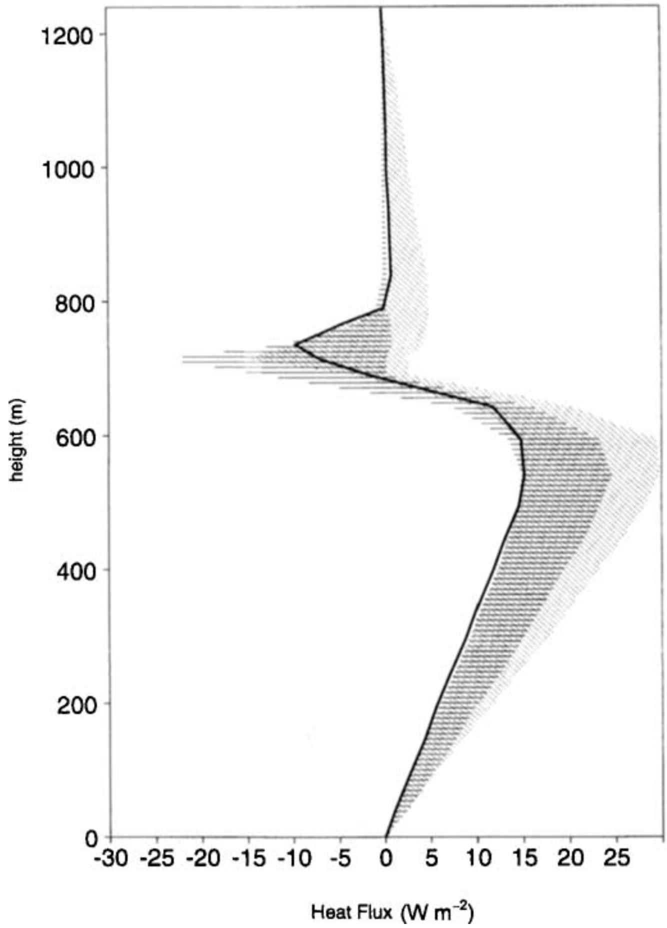

Figure 9. Comparison of total vertical heat flux in large-eddy simulation mode for the smoke-cloud against other models (adapted from Bretherton *et al.* (1999)). Thick solid line—this model output, dotted area—non-monotone advection schemes, hatched area—monotone advection schemes.

TKE (Fig. 10) has again a maximum at the inversion, probably related to the horizontal motions trapped at the interface.

(*c*) *Sheared neutral boundary layer*

We consider here the case studied by Andrén *et al.* (1994). A neutral turbulent Ekman layer at 45°N is considered, with a geostrophic wind of $(U_g, V_g) = (10, 0)$ m s^{-1} balancing the large-scale pressure gradient. A domain of ($L_x = 4000$ m, $L_y = 2000$ m, $L_z = 1500$ m) with resolutions of $\Delta x = 100$ m, $\Delta y = 50$ m, $\Delta z = 37.5$ m is used. A horizontally anisotropic grid has been chosen in view of the known elongated structures present near the wall in shear-driven boundary layers. A roughness length of $z_0 = 0.1$ m is imposed, together with an upper stress-free boundary. The height of this boundary is about $0.35u_*/f$ where u_* is friction velocity. The simulation is run for $10f^{-1}$ s, and the last $3f^{-1}$ s are used for the LES statistics.

In this case, the scale of the largest eddies is not as well defined as in the two former cases. In sheared, neutral boundary layers, the flow in the lower layer, near the surface, has a logarithmic velocity profile and friction creates the eddies whose scale increases

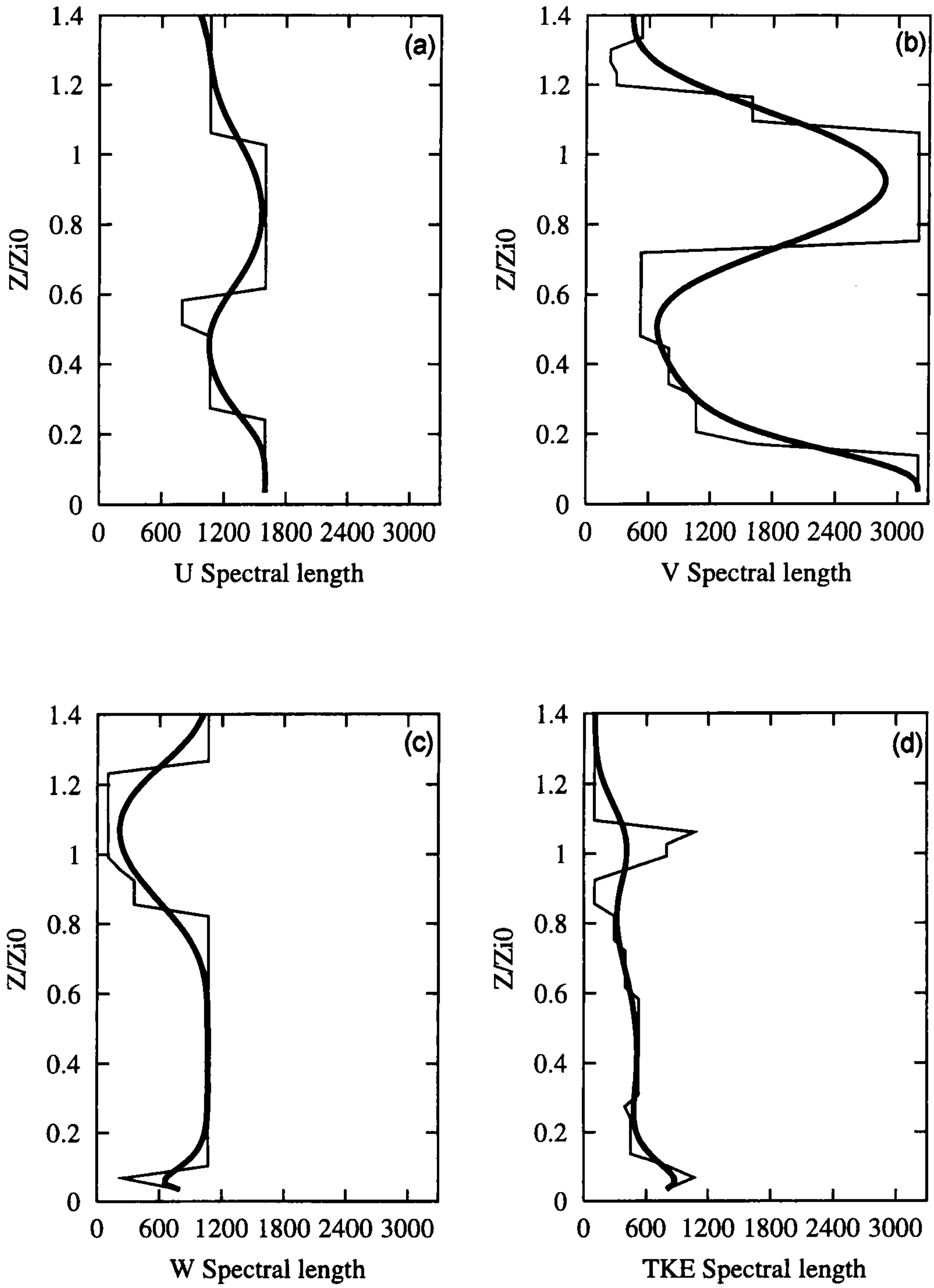

Figure 10. Vertical profiles (as in Fig. 8) of spectral lengths (m) of velocity components (a) u, (b) v and (c) w, and (d) resolved turbulent kinetic energy for the smoke-cloud case. Thick line—smoothed outputs, thin line—non-smoothed outputs.

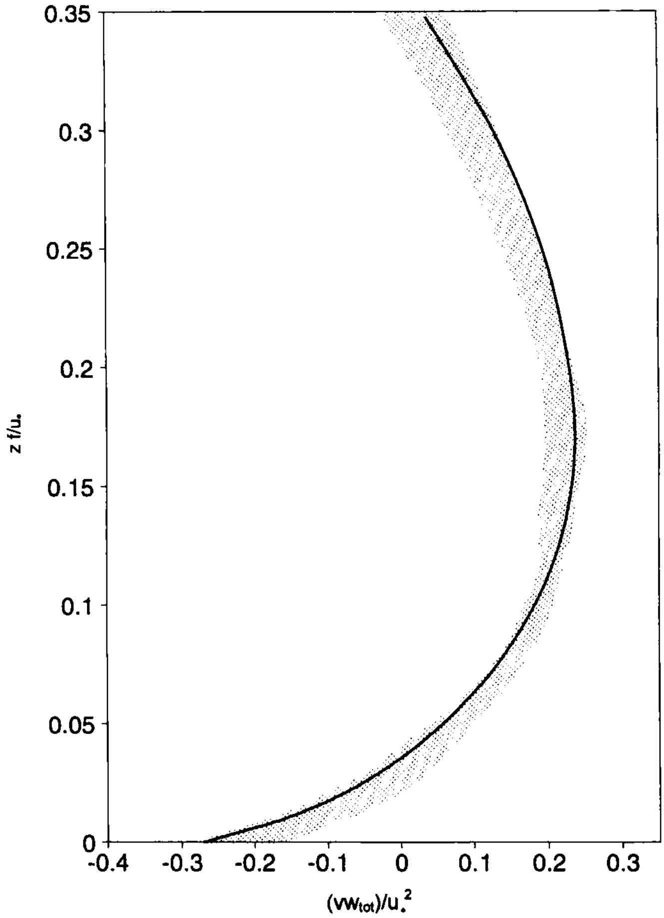

Figure 11. Comparison of total v-momentum flux in large-eddy simulation mode for the neutral boundary-layer case against data and ensemble of four other models (shaded). See text for explanation.

with height. This case is present in the atmosphere for small surface heat fluxes and strong winds, but normally limited by an inversion at some height. The dynamics of the case simulated in this section should be comparable with a real atmosphere with $\mathcal{L}/h$ greater than unity, $\mathcal{L}$ being the Monin–Obukhov length and h the inversion height. For resolutions similar to those of the former cases, a larger impact of the SGS scheme is expected, since smaller structures are present and the inertial subrange is reached at higher wave numbers.

The simulation shows that the wind component u (following the flow direction) is organized in streets elongated in the direction of the shear vector near the ground; this effect is normally attributed to the stretching by the shear of the turbulent eddies generated near the ground. The flow seems to be structured in the layers within the PBL following the surface wind direction, with eddies of around 1000 m of vertical dimension. The value of u close to the ground is around 5.5 m s^{-1}. The inspection of the v and w fields confirms the roll structure within the PBL.

The most significant mean fields are the momentum fluxes and variances. The subgrid parts are very important near the ground, decreasing smoothly with altitude (Fig. 16(d)). The intercomparison results are very similar for all the models, including the present scheme. An example is shown for the total $\langle v'w' \rangle$ flux (Fig. 11). A difference between models appears in the total variances of the horizontal components of the wind (see Andren *et al.* (1994), Fig. 5). All models, except the backscatter run, show a peak in the surface layer for the total u variance. This is also a feature of the present scheme. Following Deardorff (1972a), this might be attributed to the lack of isotropy in this semi-resolved region. Another interesting fact seen in the same figure is the local minima on the w variance at around 0.05 u_*/f, also found in our simulation.

The grid prescribed for this simulation is rather coarse and, as a result, the spectra (not shown) do not show a well-defined inertial subrange for any model. In this case, the flow is not isotropic, and the direction on which the spectra are computed is important. In this case, the x direction has been used, along the direction of the elongated streets. In consequence, the SL of u (Fig. 12) shows a maximum equal to the domain size, since the streets extend over the whole domain. The SL of v has a sharp decrease at one third of the domain, which is about the height where coherent structures loose a clear identity. The same area is significant for the SL of w, but with a maximum at the top of this layer, indicating the return motion of the eddies. This height is the same as that of the local minima of the w variance.

4. SINGLE-COLUMN RUNS COMPARED TO LES RESULTS

The vertical part of the proposed scheme must be used alone when the horizontal grid size is large enough to consider the contribution of the horizontal turbulent motions negligible. It is a subject of debate to decide what that particular grid size is for atmospheric flows, and it is very likely that it is flow dependent. In this section, we present the results obtained running in single-column mode, considering them equivalent to their effect inside a mesoscale model.

(*a*) *Convective boundary layer*

The results of the single-column run are shown in Fig. 13, compared to the total output of the HR run. The convective boundary layer (CBL) LES was performed with zero mean wind. The resolved motions generated in the LES domain are decelerated by the friction at the ground, and experience generation of resolved TKE by the shear at those levels. The height of the CBL is slightly lower than the LES (1.05 z_{i0} instead of 1.08 z_{i0}, about 50 m), perhaps related to the lack of TKE production by friction at the surface, since the parametrization is not handling the subgrid friction when a zero mean wind is prescribed. The mean θ value in the mixed layer is correct, and the profile is very close to neutral stratification, but slightly unstable. The heat flux gives an entrainment rate very close to the HR LES ($-0.15Q_s$ instead of $-0.17Q_s$). The profile in the mixed layer is linear, and shows a gentle erosion of the upper part of the inversion. The variance of temperature has correct values near the ground, but it is underestimated at the inversion (Fig. 13(d)), reaching only 30% of the LES value (normalized value of 23, while observations range from 2 to more than 50—see Stull 1988, Fig. 4.9). This difference could be explained by the presence of gravity waves over the mixed layer, observed in the LES and in many observations. Such an effect is not included in the current 1D scheme. The e profile is not far from the LES computations except near the ground, where the production by friction is not reproduced, and in the stable layer over the CBL, related to the undulations of the inversion.

Regarding the relevant parameters of the turbulence scheme, they are plotted at the top of Fig. 14. The BL89 length shows a parabolic profile with a maximum in the centre of the mixed layer. The close resemblance must be stressed here of this profile to the corresponding SL of w obtained from the LES (Fig. 8), except for a

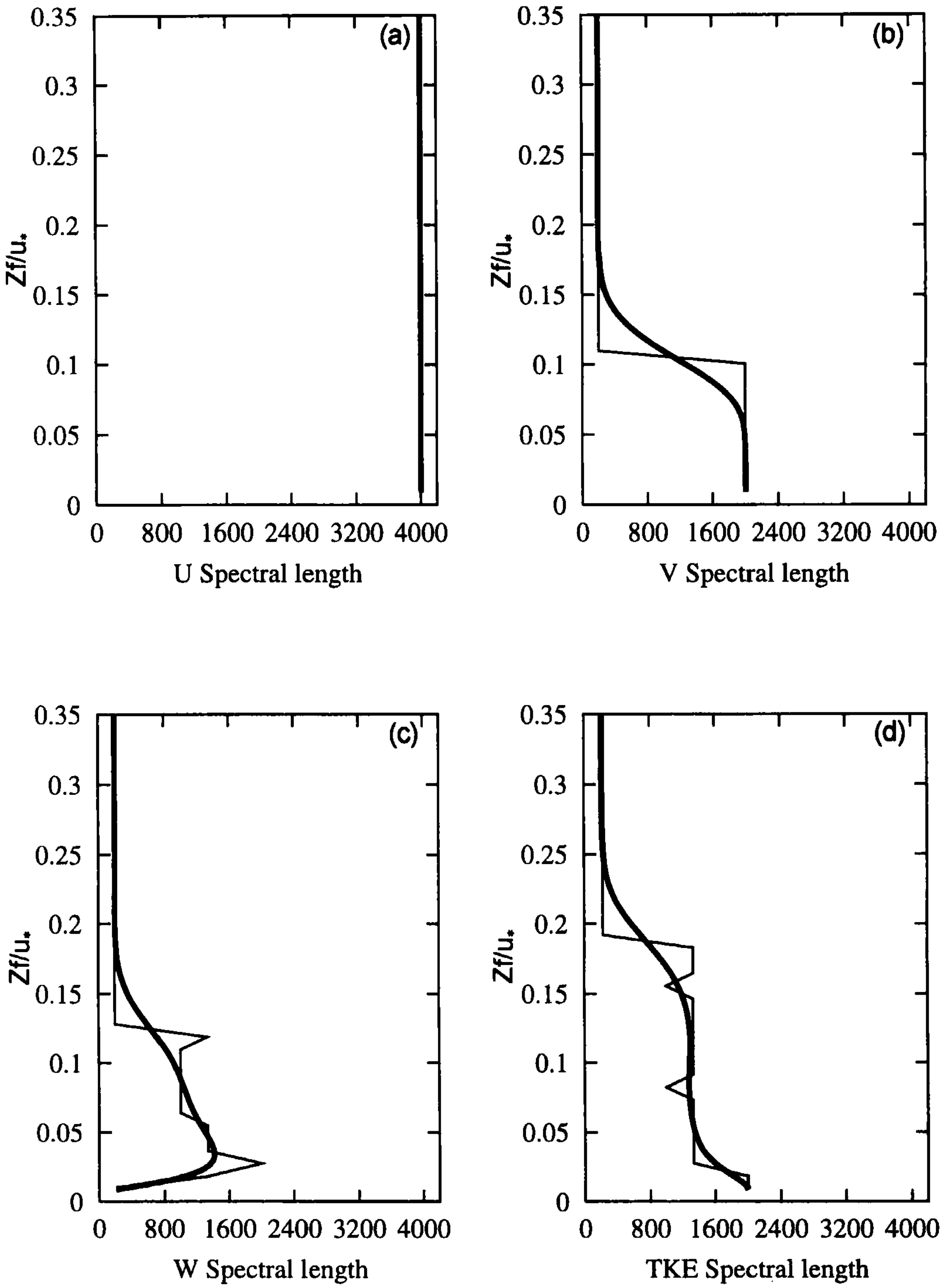

Figure 12. Vertical profiles of spectral lengths (m) of velocity components (a) u, (b) v and (c) w, and (d) resolved turbulent kinetic energy for the neutral boundary-layer case. Thick line—smoothed outputs, thin line—non-smoothed outputs.

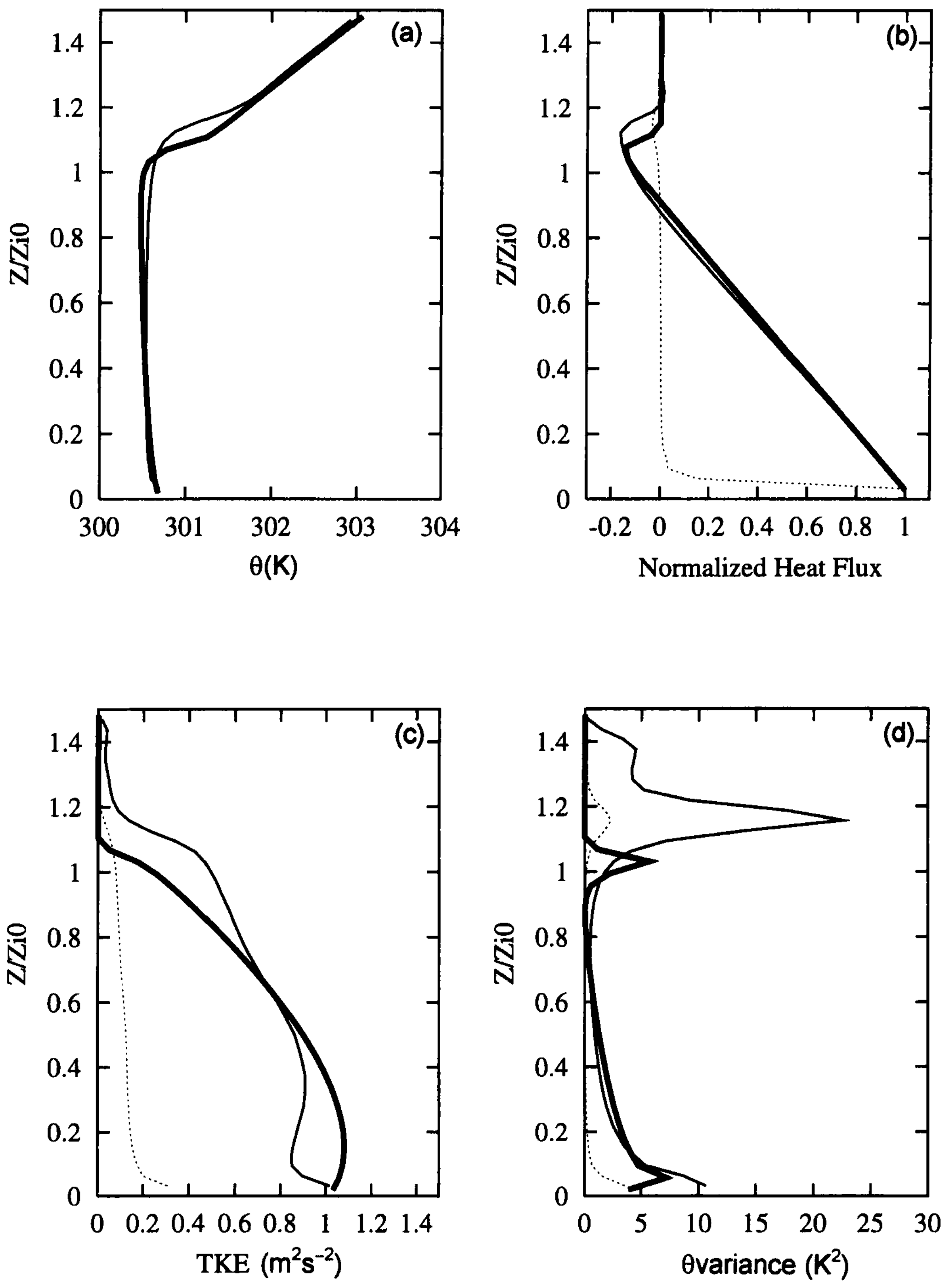

Figure 13. Comparison of 1D results with high-resolution large-eddy simulation (LES) for the convective boundary-layer case: vertical profiles of (a) potential temperature (θ), (b) vertical heat flux, (c) turbulent kinetic energy, and (d) variance of θ. Thick line—1D output, thin line—total LES output, dotted line—subgrid LES output.

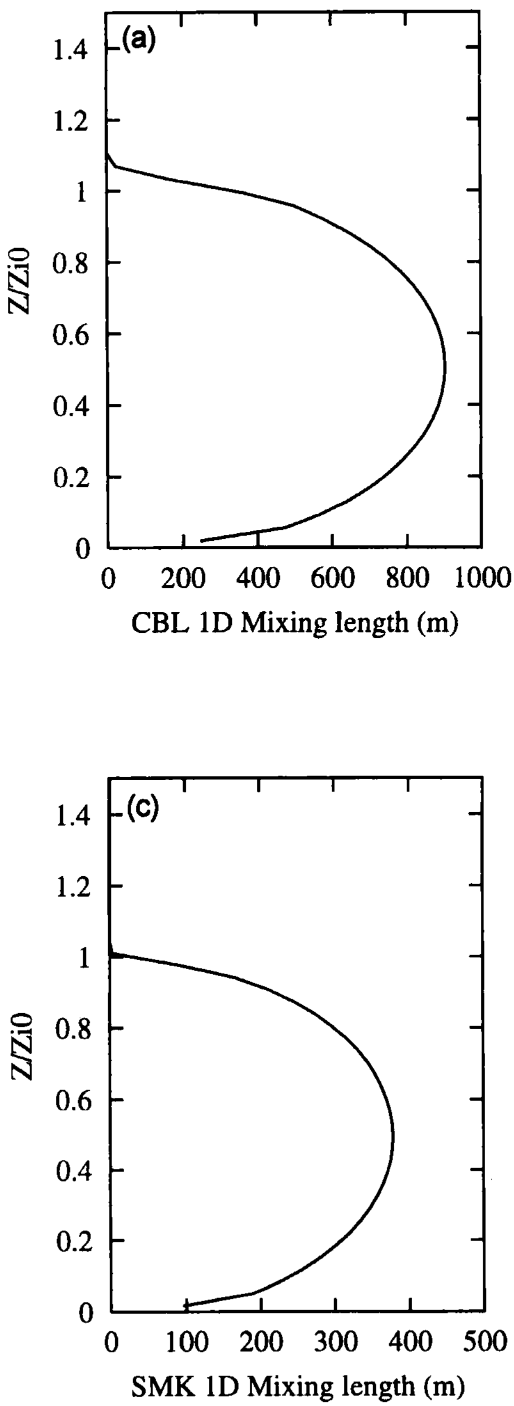

Figure 14. Vertical profiles of two relevant parameters for the 1D turbulent scheme: for the convective boundary-layer case (a) mixing length and (b) stability function (ϕ_3); for the smoke-cloud case (c) mixing length and (d) ϕ_3.

proportionality factor, suggesting that this quantity could be useful for investigating mixing-length formulations for less classical cases. The stability function ϕ_3 presents values larger than 1 in the mixed layer and takes values lower than 1 at the inversion and over, with a minimum at the entrainment layer. The mixing of temperature is thus reduced in this region by the presence of stable stratification and is less efficient than momentum mixing. In the present model, the TKE is located at the same level as θ, u and v. Therefore, we have coded a discretized prognostic equation for the TKE at the first level over the ground, and imposed the boundary condition $\overline{w'e} = 0$ at the ground, consistent with observations (see Stull (1988), Fig. 5.9). A more classic surface-layer boundary condition should be tried in the future.

(*b*) *Smoke cloud*

Results intercompared between the single-column and the averaged LES outputs are shown in Fig. 15. The correct warming and height of the boundary layer are obtained in the θ profile. The heat flux fits the LES value in the mixed layer very well, with good localization of the positive maximum (around 0.8 z_{i0}, with $z_{i0} = 730$ m). At the inversion, the heat flux has a value of -0.014 K m s^{-1} instead of -0.010 K m s^{-1} found in the LES. However, the value of the heat flux at the inversion is one of the main discrepancies in the LES intercomparison, and is therefore a very uncertain parameter. The variance $\overline{\theta'^2}$ is again smaller than the LES value, but closer to the LES value than for the CBL case. This is consistent with the good predicted value of the heat flux in the inversion. This might indicate that the gravity waves present at the inversion in this case are less intense than for the CBL LES, a reason for the values being closer between the single-column and the LES experiments. Again the TKE profile is far from the LES value close to the ground, owing to the fact that, with zero mean wind, the column model is not able to reproduce the dynamical effect of the ground. The mixing length (Fig. 14(c)) presents a maximum at the centre of the mixed layer with values close to zero in the inversion and above. It is again very close to the profile of the spectral length of w (Fig. 14(d)) and far from the SL of e. Thus, the processes taking place through the horizontal mixing at the inversion, should not be taken into account within a vertical mixing parametrization, but in a different way. The function ϕ_3 presents a maximum at the upper part of the mixed layer and leads to a very strong inhibition of mixing at the inversion.

(*c*) *Neutral boundary layer*

The classical formulation of our mixing length in single-column mode (BL89) explores the temperature field to look for limitations to the rise or fall of a particle of air. Since in this case the whole domain is neutrally stratified, $l_{\rm up}$ and $l_{\rm down}$ would be respectively equal to the distance of each computation level to the top or the bottom of the simulation domain. Since this is not a physically based parametrization, $l_{\rm down}$ is taken to be the distance to the surface (z) and $l_{\rm up}$ as the distance to the top of the turbulent domain (H), defined as the height where the TKE is under 0.01 m^{2}s^2. This results in a mixing length, taking the square root of both quantities: $L = \{z(H - z)\}^{1/2}$. The simulation with this length is able to reproduce aproximately the behaviour of the neutral sheared LES (Fig. 16). However, we expect to be able to extend BL89 to be able to treat this case correctly as well in future, probably using the spectral length profile of w computed transversally to the direction of the surface wind in the LES.

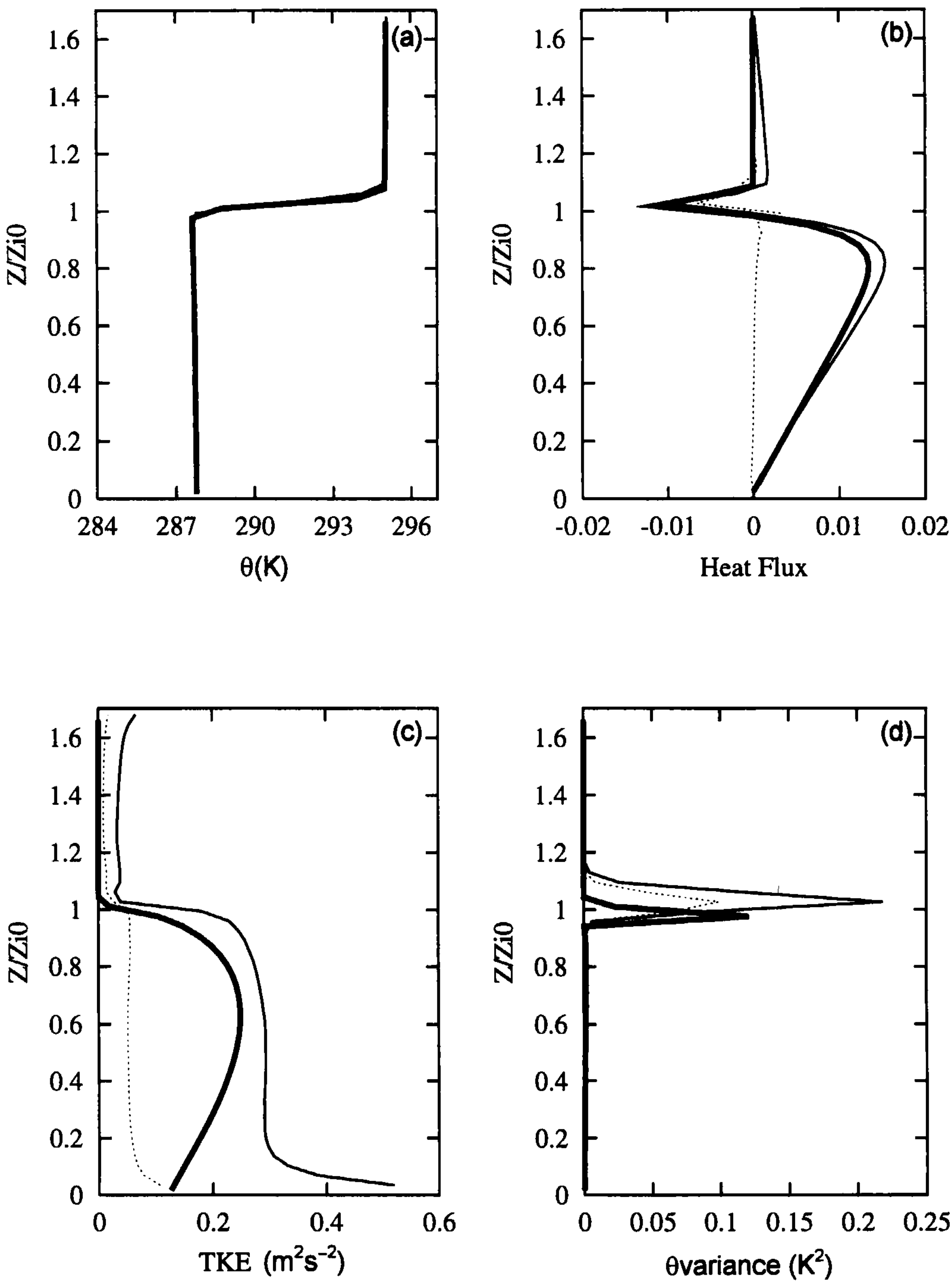

Figure 15. Comparison of 1D results with large-eddy simulation (LES) for the smoke-cloud case: vertical profiles of (a) potential temperature (θ), (b) vertical heat flux, (c) turbulent kinetic energy, and (d) variance of θ. Thick line—1D output, thin line—total LES output, dotted line—subgrid LES output.

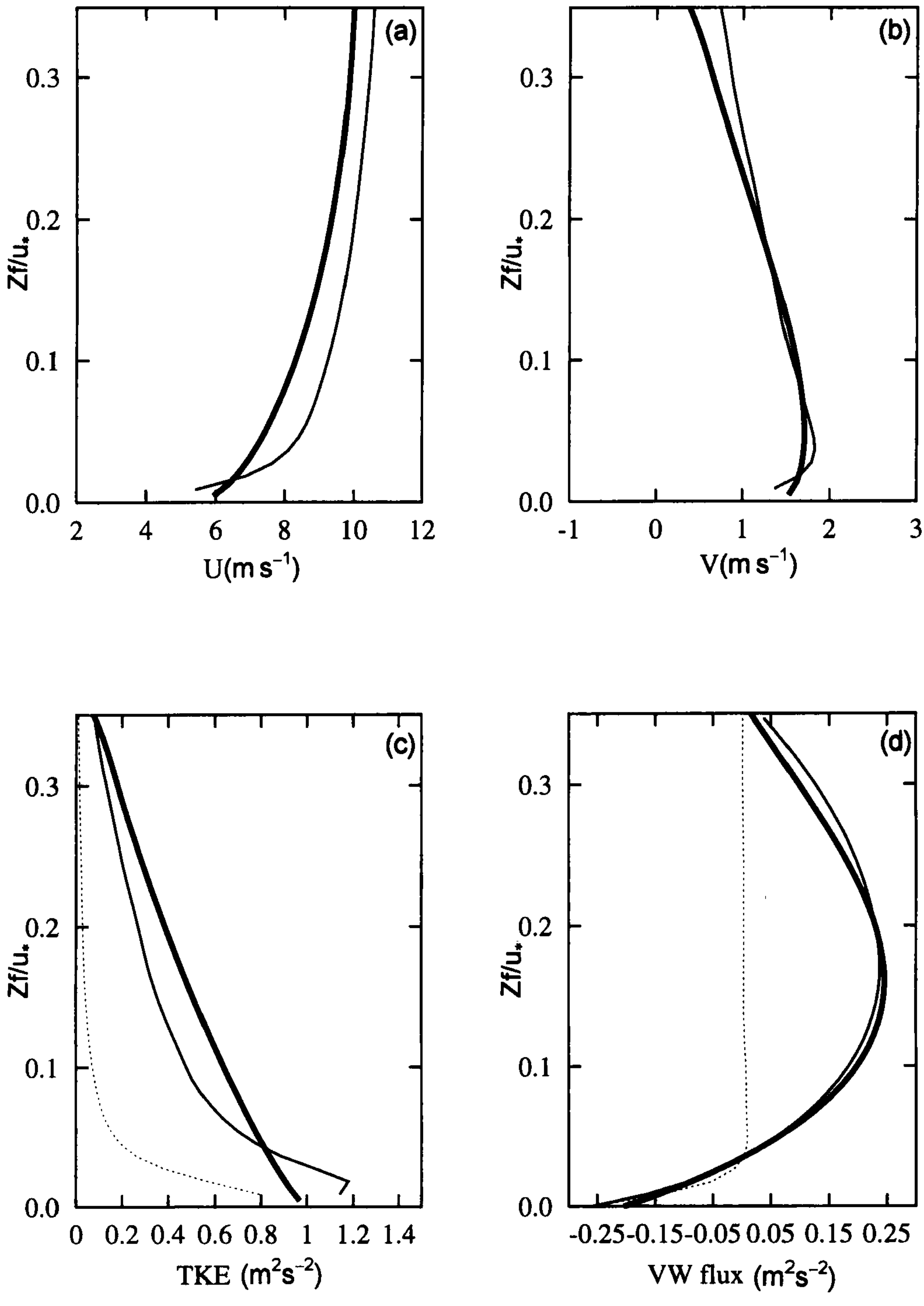

Figure 16. Comparison of 1D results with large-eddy simulation (LES) for the neutral boundary-layer case: (a) u, (b) v, (c) turbulent kinetic energy, and (d) $\overline{v'w'}$. See text for explanation of symbols. Thick line—1D output, thin line—total LES output, dotted line—subgrid LES output.

5. CONCLUSIONS

A turbulence scheme has been developed for the Meso-NH model, potentially scanning a large range of atmospheric scales. The development of the scheme was made with the objective of using it both as a subgrid-scale parametrization in LES configuration, and as a single-column parametrization in mesoscale configuration. The scheme is derived from the full set of equations for second-order moments, and uses the same set of closure constants in the LES and mesoscale configurations. A crucial hypothesis is to consider that the various length-scales introduced by the different closure problems (turbulent transport, pressure correlation and dissipation) are all proportional.

In this paper the results of the scheme have been evaluated on three classical boundary-layer regimes. A fair agreement with other LES models was found, as well as correct behaviour of the single-column mode. To our knowledge, it is the first successful experience of a single turbulence scheme running in both modes. The key to this success lies in two different factors, the formulation of the mixing length and the use of the ϕ_3 function.

The scheme differs between the LES and the single-column configuration only in the specification of the mixing length. For LES, the length is taken proportional to the grid size, implicitly assuming that the smaller explicitly simulated eddies lie in the inertial subrange of the flow. It is currently recognized that this assumption falls near solid boundaries and in strongly stably stratified layers, where the eddies are smaller than the affordable resolutions. Current work is underway to address this important issue. Another related issue for this parametrization concerns the estimation of vertical derivatives used in the prognostic equation of the turbulent kinetic energy at the first mass level. Within the stable layers, the subgrid-scale turbulent exchange of heat, moisture and passive scalars is limited by the values of the ϕ_3 function.

In single-column mode, a physically founded mixing length is used. It is based on the vertical free path of a particle displaced up to its neutral buoyancy level. This allows the expected turbulent fluxes (from LES and observations) to be obtained. A limitation occurs in a pure neutral case, where the particle always travels to the limits of the domain. In that case we imposed a parabolic length in the area where the turbulent kinetic energy was larger than a minimum value, with successful results. Although the later procedure is purely ad hoc, that should not to be considered as a large limiting factor for future use of the scheme, as this case is never encountered in the real atmosphere. As long as the PBL is topped by a stable zone as in reality, the usual formulation of the mixing length supplies an adequate result.

Furthermore we have investigated the behaviour of the spectrum of energy in our LES simulations, and deduced the size of the energetic eddies (the so-called spectral length). The profiles of the parametrized length closely resemble the profiles obtained from the LES simulations for w. These spectral analyses should be extended in the future to provide hints for deriving mixing and dissipation lengths.

The other originality of the scheme is the use of the ϕ_3 stability function; ϕ_3 enhances the mixing in unstably stratified layers and reduces it in the stably stratified ones. It is rigorously derived from the second-order system of equations instead of being an ad hoc stability function. The heat flux can be rewritten expanding the ϕ_3 formulation in 1D mode leading to a formulation very close to that proposed by Deardorff for the counter-gradient.

The combination of the parametrized length-scale with the ϕ_3 function, used for the first time in single-column simulations, did supply good results.

An issue to be further explored is the ground boundary condition. At present, a prognostic equation is used for the turbulent kinetic energy in the first model level. This makes its value very dependent on how the wind values are forced at the surface. This is especially important for the zero mean-wind cases, where the subgrid friction should be parametrized explicitly. No conclusive results have been obtained using a similarity expression for the TKE at this level, but more work should be devoted to this problem.

The present scheme is easily applicable to cloudy boundary layers using conservative variables for non-precipating processes, liquid-water potential temperature and total water. This work is in progress and a first use can be found in Duynkerke *et al.* (1999), where the model has been applied for a stratocumulus deck both in single-column mode and in LES with satisfactory results.

ACKNOWLEDGEMENTS

Special thanks to Joel Stein (Météo-France/CNRM/GMME) for all his help in implementing the scheme within the Meso-NH model. J. Cuxart is partially funded by Contract ERBCHBGCT920232 of the HCM program of the Commission of European Communities.

REFERENCES

Andrén, A., Brown, A. R., Graf, J., Mason, P. J., Moeng, C.-H., Nieuwstadt, F. T. M. and Schumann, U.	1994	Large-eddy simulation of a neutrally stratified boundary layer: A comparison of four computer codes. *Q. J. R. Meteorol. Soc.*, **120**, 1457–1484
Arya, S. P. S.	1972	The critical condition for the maintenance of turbulence in stratified flows. *Q. J. R. Meteorol. Soc.*, **98**, 264–273
Bougeault, P. and Lacarrère, P.	1989	Parameterization of orography-induced turbulence in a mesobeta-scale model. *Mon. Weather Rev.*, **117**, 1872–1890
Bretherton, C. S., Macvean, M., Bechtold, P., Chlond, A., Cotton, W., Cuxart, J., Cuijpers, H., Khairoutdinov, M., Kosovic, B., Lewellen, D., Moeng, C-H., Siebesma, P., Stevens, B., Stevens, D., Sykes, I. and Wyant, M.	1999	An intercomparison of radiatively driven entrainment and turbulence in a smoke-cloud, as simulated by different numerical models. *Q. J. R. Meteorol. Soc.*, **125**, 391–424
Brost, R. A. and Wyngaard, J. C.	1978	A model study of the stably stratified planetary boundary layer. *J. Atmos. Sci.*, **35**, 1427–1440
Canuto, V. M., Minotti, F., Ronchi, C., Ympa, R.M. and Zeman, O.	1994	Second-order closure PBL model with new third-order moments: Comparison with LES data. *J. Atmos. Sci.*, **51**, 1605–1618
Cuijpers, J. W. M. and Holtslag, A. A. M.	1998	Impact of skewness and nonlocal effects on scalar and buoyancy fluxes in convective boundary layers. *J. Atmos. Sci.*, **55**, 151–162
Cuxart, J.	1997	'Planetary boundary layer simulation: From LES to general circulation models'. PhD Thesis, Universitat de Barcelona
Cuxart, J., Bougeault, P., Lacarrère, P., Noilhan, J. and Soler, M. R.	1994	A comparison between transilient turbulence theory and the exchange coefficient model approaches. *Boundary-Layer Meteorol.*, **67**, 251–276
Deardorff, J. W.	1972a	Numerical investigation of neutral and unstable planetary boundary layers. *J. Atmos. Sci.*, **29**, 91–115
	1972b	Theoretical expression for the countergradient vertical heat flux. *J. Geophys. Res.*, **30**, 5900–5904
	1973	Three-dimensional numerical modeling of the planetary boundary layer. Pp. 273–311 in proceedings of Workshop on micrometeorology, Boston, August 1973. Ed. D. A.Haugen. American Meteorological Society
	1980	Stratocumulus-capped mixed layers derived from a three-dimensional model. *Boundary-Layer Meteorol.*, **18**, 495–527

Duynkerke, P. G., Jonker, P. J., Chlond, A., van Zanten, M. C., Cuxart, J., Clark, P., Sanchez, E., Martin, G., Lenderink, G. and Teixeira, J. 1999 Intercomparison of three- and one-dimensional model simulations and aircraft observations of stratocumulus. *Boundary-Layer Meteorol.* (in press)

Holtslag, A. A. M. and Boville, B. A. 1993 Local versus nonlocal boundary-layer diffusion in a global climate model. *J. Climate* **6**, 1825–1842

Holtslag, A. A. M. and Moeng, C.-H. 1991 Eddy diffusivity and countergradient transport in the convective atmospheric boundary layer. *J. Atmos. Sci.*, **48**, 1690–1698

Kolmogorov, A. N. 1942 Equations of turbulent motion of an incompressible fluid. *Izv. Akad. Nauk, SSSR, Ser. Fiz. Vl.* **1-2**, 56–58

Krettenauer, K. and Schumann, U. 1992 Numerical simulation of turbulent convection over wavy terrain. *J. Fluid Mech.*, **237**, 261–299

Lafore, J. P., Stein, J., Asencio, N., Bougeault, P., Ducrocq, V., Duron, J., Fischer, C., Hereil, P., Mascart, P., Pinty, J. P., Redelsperger, J. L., Richard, E. and Vila-Guerau de Arellano, J. 1998 The Meso-NH atmospheric simulation system. Part I: Adiabatic formulation and control simulation. *Annales Geophysicae*, **16**, 90–109

Leith, C. E. 1990 Stochastic backscatter in a subgrid-scale model: Plane shear mixing layer. *Phys. Fluids A*, **2**, 297–299

Lilly, D. K. 1962 On the numerical simulation of buoyant convection. *Tellus*, **14**, 148–172

1967 'The representation of small-scale turbulence in numerical simulation experiments'. Pp. 195–209 in proceedings of the IBM scientific computing symposium on environmental sciences. Yorktown Heights, USA, November 1967

Louis, J. F. 1979 A parametric model of vertical eddy fluxes in the atmosphere. *Boundary-Layer Meteorol.*, **17**, 187–202

Mason, P. J. and Thomson, D. J. 1992 Stochastic backscatter in large-eddy simulations of boundary layers. *J. Fluid Mech.*, **242**, 51–78

Mellor, G. L. and Yamada, T. 1974 A hierarchy of turbulence closure models for planetary boundary layers. *J. Atmos. Sci.*, **31**, 1791–1806

1982 Development of a turbulence closure model for geophysical fluid problems. *Rev. Geophys. Space Phys.*, **20**, 851–875

Nieuwstadt, F. T. M., Mason, P. J., Moeng, C.-H. and Schumann, U. 1993 Large-eddy simulation of the convective boundary layer: A comparison of four computer codes. Pp. 343–367 in *Turbulence Shear Flows 8*, Springer-Verlag

Redelsperger, J.-L. and Sommeria, G. 1981 Méthode de représentation de la turbulence d'échelle inférieure à la maille pour un modèle tri-dimensionnel de convection nuageuse. *Boundary-Layer Meteorol.*, **21**, 509–530

1986 Three-dimensional simulation of a convective storm: Sensitivity studies on subgrid parameterization and spatial resolution. *J. Atmos. Sci.*, **43**, 2619–2635

Schmidt, H. and Schumann, U. 1989 Coherent structure of the convective boundary layer derived from large-eddy simulations. *J. Fluid Mech.*, **200**, 511–562

Schumann, U. 1991 Subgrid length-scales for large-eddy simulation of stratified turbulence. *Theor. Comput. Fluid Dynamics*, **2**, 279–290

Smagorinsky, J. 1963 General circulation experiments with the primitive equations. Part I: The basic experiment. *Mon. Weather Rev.*, **91**, 99–164

Sommeria, G. 1976 Three-dimensional simulation of turbulent processes in an undisturbed trade wind boundary layer. *J. Atmos. Sci.*, **33**, 216–241

Stull, R. B. 1988 *An introduction to boundary layer meteorology*. Kluwer Academic Publishers, Amsterdam

Sullivan, P. P., McWilliams, J. C. and Moeng, C.-H 1994 Subgrid-scale model for large-eddy simulation of planetary boundary-layer flows. *Boundary-Layer Meteorol.*, **71**, 247–276

Thérry, G. and Lacarrère, P. 1983 Improving the eddy kinetic energy model for planetary boundary layer description. *Boundary-Layer Meteorol.*, **25**, 63–68

Yagüe, C. and Cano, J. L. 1994 Eddy transfer processes in the atmospheric boundary layer. *Atmos. Env.*, **28**, 1275–1289